

Calibrating multi-dimensional complex ODE from noisy data via deep neural networks

Kexuan Li

Global Analytics and Data Sciences, Biogen Inc

Fangfang Wang

Department of Mathematical Science, Worcester Polytechnic Institute

Ruiqi Liu

Department of Mathematics and Statistics, Texas Tech University

Fan Yang

Eli Lilly and Company

Zuofeng Shang

Department of Mathematical Sciences, New Jersey Institute of Technology

September 20, 2023

Abstract

Ordinary differential equations (ODEs) are widely used to model complex dynamics that arise in biology, chemistry, engineering, finance, physics, etc. Calibration of a complicated ODE system using noisy data is generally challenging. In this paper, we propose a two-stage nonparametric approach to address this problem. We first extract the de-noised data and their higher order derivatives using boundary kernel method, and then feed them into a sparsely connected deep neural network with rectified linear unit (ReLU) activation function. Our method is able to recover the ODE system without being subject to the curse of dimensionality and the complexity of the ODE structure. We have shown that our method is consistent if the ODE possesses a general modular structure with each modular component involving only a few input variables, and the network architecture is properly chosen. Theoretical properties are corroborated by an extensive simulation study that also demonstrates the effectiveness of the proposed method in finite samples. Finally, we use our method to simultaneously characterize the growth rate of COVID-19 cases from the 50 states of the United States.

Keywords: Deep neural networks; Ordinary differential equations; ReLU activation function; Feature selection.

1 Introduction

The use of ordinary differential equations (ODEs) is prevalent in both social and natural sciences to study complex dynamic phenomena or dynamical systems. For instance, linear ODEs are often used to describe population growth (Henderson and Loreau (2019)), Lorenz equation—a high-dimensional nonlinear ODE system—widely used to characterize chaos systems (Talwar and Namachchivaya Sri (1992)), and high-dimensional linear ODEs used to construct a dynamic gene regulatory network (Lu et al. (2011)). Therefore, calibrating complicated ODE systems is of great interest and importance to both theorists and practitioners.

Owing to the superior performance of deep learning in modeling complicated data, deep neural networks have been actively used to reproduce dynamical systems (Weinan (2017)). Deep neural networks, such as residual network (He et al. (2016)) and discrete normalizing flows (Kobyzev et al. (2020)), can be considered as discrete dynamical systems. Recently, Chen et al. (2018) propose a new family of continuous neural networks that extend the traditional discrete sequence of hidden layers to continuous-depth by using an ODE to parameterize the hidden units. Lusch et al. (2018) and Champion et al. (2019) consider an autoencoder-based architecture to understand and predict complex dynamical systems.

Despite advances in deep learning, most of the existing methods lack interpretability and their theoretical underpinnings are not well grounded. In this paper, we attempt to fill the gap and provide statistical justification for calibrating a complex system that can be characterized by multi-dimensional nonlinear ODEs. In particular, we are interested in scenarios where data, collected from continuous-time nonlinear ODEs, are asynchronized, irregularly spaced and are contaminated by measurement errors.

To start with, consider the following multi-dimensional ν th order ODE system in its general form:

$$\frac{d^\nu}{dt^\nu} \mathbf{x}(t) = \mathbf{f}_0(\mathbf{x}(t), \mathbf{x}^{(1)}(t), \dots, \mathbf{x}^{(\nu-1)}(t)), \quad 0 \leq t \leq 1, \quad (1)$$

where $\mathbf{x}(t) = (x_1(t), \dots, x_d(t))^\top \in \mathbb{R}^d$ and $\mathbf{x}^{(j)}(t)$ represents the j th derivative of $\mathbf{x}(t)$. With $r_0 = \nu d$, $\mathbf{f}_0(\cdot) = (f_{0,1}(\cdot), \dots, f_{0,d}(\cdot))^\top : \mathbb{R}^{r_0} \rightarrow \mathbb{R}^d$ is a d -dimensional function of $\mathbf{x}(t), \mathbf{x}^{(1)}(t), \dots, \mathbf{x}^{(\nu-1)}(t)$, and it represents the unknown ground-truth, characterizing the interactions among $\mathbf{x}(t), \mathbf{x}^{(1)}(t), \dots, \mathbf{x}^{(\nu-1)}(t)$. When $\nu = 1$, (1) degenerates to a first order ODE system:

$$\frac{d}{dt} \mathbf{x}(t) = \mathbf{f}_0(\mathbf{x}(t)), \quad 0 \leq t \leq 1. \quad (2)$$

Suppose that the d -dimensional continuous-time process $\mathbf{x}(t)$ is observed at discrete and possibly asynchronous time points; that is, $x_j(t)$ is observed at $0 \leq t_{j1} < t_{j2} < \dots < t_{jn_j} \leq 1$,

$j = 1, \dots, d$. It is common that the collected data are contaminated by measurement error. Therefore, we use y_{ji} to denote the data point we observe at time t_{ji} and it relates to $x_j(t_{ji})$ in the following way:

$$y_{ji} = x_j(t_{ji}) + \epsilon_{ji}, \quad i = 1, \dots, n_j, \quad j = 1, \dots, d, \quad (3)$$

where $\epsilon_{ji} \sim N(0, \sigma_j^2)$ represents the measurement error at time t_{ji} . The time stamps are allowed to be irregularly spaced and asynchronous, thereby, yielding different sample sizes n_j for different components j . The statistical task is to estimate the multi-dimensional nonlinear function \mathbf{f}_0 in (1) using the observed noisy data $\{\mathbf{y}_1, \dots, \mathbf{y}_d\}$, where $\mathbf{y}_j = (y_{j1}, \dots, y_{jn_j})^\top$. It is worthwhile to mention that our goal is to estimate \mathbf{f}_0 as a function of $\mathbf{x}(t), \mathbf{x}^{(1)}(t), \dots, \mathbf{x}^{(\nu-1)}(t)$, not a function of t .

In general, it is computationally cumbersome to estimate \mathbf{f}_0 via conventional nonparametric techniques. To avoid this, we utilize deep neural networks and propose a two-stage nonparametric estimation procedure. In Stage 1, we use kernel approach to filter out the noise in $\{\mathbf{y}_1, \dots, \mathbf{y}_d\}$ and obtain consistent estimators of $\mathbf{x}(t)$ and its high order derivatives $\mathbf{x}^{(j)}(t)$, denoted by $\hat{\mathbf{x}}(t)$ and $\hat{\mathbf{x}}^{(j)}(t)$, $j = 1, 2, \dots, \nu$, respectively (see Section 3.1). In Stage 2, we adopt a ReLU feedforward neural network to approximate $\hat{\mathbf{x}}^{(\nu)}(t)$. By assuming that the function $\mathbf{f}_0(\cdot)$ enjoys a general modular structure with each modular component involving only a few input variables, we establish the consistency of the rectified linear unit (ReLU) feedforward neural network estimator and derive its convergence rate. In particular, we show that the rate is not subject to the dimension of the ODE system, but depends solely on the length and width of the neural network $\hat{\mathbf{f}}(\cdot)$ and the smoothness of the function $\mathbf{f}_0(\cdot)$ (See Section 3.2). As pointed out by Hartford et al. (2017), DNN is more computationally tractable than conventional nonparametric methods such as spline methods in the scenarios with high-dimensional features.

In light of (1), each component of $\mathbf{x}(t)$ satisfies

$$\frac{d^\nu}{dt^\nu} x_j(t) = f_{0,j}(\mathbf{x}(t), \mathbf{x}^{(1)}(t), \dots, \mathbf{x}^{(\nu-1)}(t)), \quad 0 \leq t \leq 1, \quad (4)$$

for $j = 1, \dots, d$. Oftentimes the inputs, $\mathbf{x}(t), \mathbf{x}^{(1)}(t), \dots, \mathbf{x}^{(\nu-1)}(t)$, do not contribute equally to $x_j^{(\nu)}(t)$. In some applications, the governing function $f_{0,j}$ is sparsely represented; in other words, only a small subset of the inputs $(x_1(t), \dots, x_d(t), x_1^{(1)}(t), \dots, x_d^{(1)}(t), \dots, x_1^{(\nu-1)}(t), \dots, x_d^{(\nu-1)}(t))$ is associated with $x_j^{(\nu)}(t)$. For example, biologists might have interest in recovering gene regulatory networks from noisy expression data where the cell regulation is only associated with a small set of genes. In such cases, it is critical to learn the governing equations as well as the associated coordinate system simultaneously. Based on the interactions between feature (or variable) selection search and the learning model, traditional feature selection methods fall into three broad

categories: filter methods, wrapper methods, and embedded methods. However, successful applications of these classical methods in the ODE setting are limited unless the ODE system is linear or parametric, or contains only lower order derivatives. Recently, Lemhadri et al. (2021) introduces a new neural network framework called LassoNet, which can capture the nonlinearity in $f_{0,j}$ nonparametrically with global feature selection. Motivated by the superior performance of LassoNet, we present an accurate and computational feasibility method that is capable of identifying relevant input variables in (4) after estimating $\mathbf{x}(t)$ and its derivatives from noisy data.

The rest of the paper is organized as follows. In Section 2, we review some related work on governing equation estimation and variable selection in ODE systems, and point out where our work stands in the literature. Section 3 details the proposed method as well as its theoretical properties. In Section 4, we conduct simulation study to assess the theoretical findings. An application to the COVID cases is presented in Section 5. Section 6 concludes the paper. All the proofs are collected in the supplementary material.

Terminologies and Notation: In this paper all vectors are column vectors. For two positive sequences $\{a_n\}$ and $\{b_n\}$, we say $a_n \lesssim b_n$ if there exists a positive constant c such that $a_n \leq cb_n$ for all n , and $a_n \asymp b_n$ if $c^{-1}a_n \leq b_n \leq ca_n$ for some constant $c > 1$ and a sufficiently large n . For $\mathbf{x} = (x_1, \dots, x_d)^\top$, let $\|\mathbf{x}\|_2^2 = \mathbf{x}^\top \mathbf{x}$, $|\mathbf{x}| = (|x_1|, \dots, |x_d|)$, $|\mathbf{x}|_\infty = \max_{i=1, \dots, d} |x_i|$, and $|\mathbf{x}|_0 = \sum_{i=1}^d \mathbb{1}(x_i \neq 0)$, where $\mathbb{1}(\cdot)$ is the indicator function. For two d -dimensional vectors $\mathbf{x} = (x_1, \dots, x_d)^\top$ and $\mathbf{y} = (y_1, \dots, y_d)^\top$, we say $\mathbf{x} \lesssim \mathbf{y}$ if $x_i \lesssim y_i$, for $i = 1, \dots, d$. For an $n \times n$ matrix $A = (a_{i,j})_{n \times n}$, let $\|A\|_\infty = \max_{i,j=1, \dots, n} |a_{ij}|$ be the max norm of A and $\|A\|_0$ be the number of non-zero entries of A . Let $\|f\|_2^2 = \int f(x)^2 dx$ the L_2 norm of a real-valued function f and $\|\mathbf{f}\|_\infty$ the sup-norm for a d -dimensional function \mathbf{f} . We use $\lfloor x \rfloor$ to represent the largest number less than x and $\lceil x \rceil$ the smallest number greater than x , and use $a \wedge b$ and $a \vee b$ to represent the minimum and maximum of two numbers a and b , respectively.

2 Related Work

In a parametric/semi-parametric setting where $\mathbf{f}_0(\cdot)$ is parameterized, the process of estimating the unknown parameters in \mathbf{f}_0 is the so-called inverse problem and has been widely studied in statistical literature. For example, consider the first order ODE system in (2) and suppose that it involves an unknown parameter θ , i.e., $\frac{d\mathbf{x}(t;\theta)}{dt} = \mathbf{f}_0(\mathbf{x}(t;\theta); \theta)$. It has been discussed in, among other, Benson (1979) and Biegler et al. (1986) that θ can be consistently estimated by the least square estimator provided that the data are collected regularly and synchronously over time, i.e.,

$n_1 = n_2 = \dots = n_d = n$ and $t_{1i} = t_{2i} = \dots = t_{di}$ for $i = 1, \dots, n$:

$$\hat{\theta}_{LSE} = \underset{\theta}{\operatorname{argmin}} \sum_{i=1}^n \sum_{j=1}^d (y_{ji} - x_j(t_{ji}))^2.$$

If the measurement errors ϵ_{ji} are normally distributed, then $\hat{\theta}_{LSE}$ coincides with the maximum likelihood estimator and is \sqrt{n} -consistent. Unfortunately, in most cases, $\hat{\theta}_{LSE}$ has no closed-form expression and tends to be computationally expensive. To overcome this issue, many other methods have been developed; see Liang and Wu (2008), Hall and Ma (2014), Bhaumik and Ghosal (2015), Wu et al. (2019), and Sun et al. (2020), to name a few. However, they all suffer from the curse of dimensionality and can only deal with lower order derivatives.

In cases where \mathbf{f}_0 cannot be summarized by a few low-dimensional parameters, calibrating \mathbf{f}_0 becomes more demanding. Existing solutions attempt to impose extra assumptions in order to simplify the structure of \mathbf{f}_0 . For instance, Henderson and Michailidis (2014) and Chen et al. (2017) assume an additive structure on \mathbf{f}_0 , while Paul et al. (2016) considers \mathbf{f}_0 to be positive. To well preserve the structure of \mathbf{f}_0 so as to align with what is observed in practice, we suggest a two-stage deep learning based method that estimates \mathbf{f}_0 nonparametrically by imposing a general modular structure on \mathbf{f}_0 with each modular component involving only a few input variables. This method can handle higher order derivatives and recover the ODE system without being subject to the curse of dimensionality.

Statistical literature on variable selection in the context of ODE system largely focuses on linear, low dimensional, or lower order derivative ODE. For example, Zhang et al. (2015) only consider the first order derivative and estimate the governing function \mathbf{f}_0 as a linear combination of basis functions. In the work of Chen et al. (2017), the authors also assume the derivative is only first order and the right-hand side of (4) is additive, that is $f_{0,j} = \theta_{j,0} + \sum_{k=1}^d f_{0,j,k}(x_k(t))$ for some $\theta_{0,j} \in \mathbb{R}$. Recently, Wu et al. (2019) propose a new parameter estimation and variable selection method based on similarity transformation and separable least squares for large-scale systems; however, their approach can only be used in homogeneous linear system. Identifying relevant features for multi-dimensional complex ODE remains an open challenge.

Recently, deep neural network has been successfully applied in many fields, such as computer vision (He et al., 2016), natural language processing (Bahdanau et al., 2014), survival analysis (Li, 2022), bioinformatics (Min et al., 2017), recommendation systems (Zhang et al., 2019), spatial statistics (Li et al., 2023), and variable selection (Lemhadri et al., 2021; Li et al., 2023). Investigating theoretical properties of deep neural network is also of great interest to many statisticians and data scientists alike. In the statistical literature, Schmidt-Hieber (2020) proves that using

sparingly connected deep neural networks with ReLU activation function can achieve the mini-max rate of convergence in a nonparametric setting. Farrell et al. (2021) obtains convergence rates similar to Schmidt-Hieber (2020) under different regularity conditions. Similarly, Bauer and Kohler (2019) shows that multilayer feed-forward neural networks are able to circumvent the curse of dimensionality if the ground-truth \mathbf{f}_0 satisfies a generalized hierarchical interaction model. A theoretical understanding of deep learning can also be achieved through approximation theory; for example, see Li et al. (2019), Hammer (2000), Li et al. (2020), Elbrächter et al. (2021), Lu et al. (2021). Unlike the traditional function approximation theory that uses the aggregation of simple functions to approximate complicated ones, deep neural networks use the compositions of simple functions, which motivates us to assume that the function \mathbf{f}_0 satisfies a compositional structure.

3 Methodology and Main Theorem

In this section, we shall detail the two-stage estimation procedure and provide its theoretical underpinnings. We also present a variant of the Stage-2 estimator to achieve variable selection in the context of ODE systems.

3.1 Stage 1: Kernel Estimator

Our goal in the first stage is to estimate $\mathbf{x}(t) = (x_1(t), \dots, x_d(t))^\top$ and its ν th derivative $\mathbf{x}^{(\nu)}(t)$, $\nu \geq 1$, for $0 \leq t \leq 1$, on the basis of the noisy observations $\{\mathbf{y}_1, \dots, \mathbf{y}_d\}$. This is achieved via kernel estimation by casting (3) as a nonparametric regression.

The classical kernel estimator of $x_j(t)$, $j = 1, \dots, d$, is given by

$$\tilde{x}_j(t) = \sum_{i=1}^{n_j} \frac{t_{ji} - t_{j(i-1)}}{h_j} K\left(\frac{t - t_{ji}}{h_j}\right) \cdot y_j(t_{ji}),$$

where $t_{j0} = 0$ and h_j is a sequence of positive bandwidths satisfying $h_j \rightarrow 0$ and $n_j h_j \rightarrow \infty$ as $n_j \rightarrow \infty$, and $K(\cdot)$ is a non-negative Lipschitz continuous kernel function satisfying

$$\int_{-\infty}^{\infty} K(x) dx = 1, \quad \int_{-\infty}^{\infty} (K(x))^2 dx < \infty. \quad (5)$$

Despite that $\tilde{x}_j(t)$ is consistent for $x_j(t)$ for $t \in (0, 1)$ (see Priestley and Chao (1972)), the classical kernel estimator does not lead to a consistent estimator of $x_j^{(\nu)}(t)$. Therefore, we adopt the boundary kernel function introduced in Gasser and Müller (1984) here.

We first estimate $x_j(t), j = 1, \dots, d$, by

$$\widehat{x}_j(t) = \frac{1}{h_j} \sum_{i=1}^{n_j} \int_{s_{i-1}}^{s_i} K\left(\frac{t-u}{h_j}\right) du \cdot y_j(t_{ji}), \quad (6)$$

where $0 = s_0 \leq s_1, \dots, \leq s_{n_j} = 1$, $s_i \in [t_{ji}, t_{j(i+1)}]$, $i = 1, \dots, n_j - 1$, h_j is a sequence of positive bandwidths satisfying $h_j \rightarrow 0$ and $n_j h_j \rightarrow \infty$ as $n_j \rightarrow \infty$. Moreover, $K(\cdot)$ is a ν times differentiable kernel function that has a compact support on $[-\tau, \tau]$ with $K(-\tau) = K(\tau) = 0$ and fulfills (5), and its ν th derivative, K_ν , meets the following requirements:

- (i) The support of K_ν is $[-\tau, \tau]$ and $\int_{-\tau}^{\tau} K_\nu(x) dx = 1$;
- (ii) For constants $\beta \in \mathbb{R}$ and $k \geq \nu + 2$,

$$\int_{-\tau}^{\tau} K_\nu(x) x^j dx = \begin{cases} 0 & j = \{0, \dots, k-1\} \setminus \nu, \\ (-1)^\nu \nu!, & j = \nu, \\ \beta, & j = k. \end{cases} \quad (7)$$

In order to obtain a consistent estimator of $\mathbf{x}^{(\nu)}(t)$ for $t \in [0, 1]$, i.e., to eliminate boundary effects that become prominent when estimating derivatives, we introduce the modified kernel $K_{\nu,q}$ with support $[-\tau, q\tau]$, for some $q \in [0, 1]$, satisfying $K_{\nu,q} \rightarrow K_\nu$ as $q \rightarrow 1$. Moreover, $K_{\nu,q}(x)$ satisfies (7) with a uniformly bounded k -th moment for q , and the asymptotic variance of $K_{\nu,q}$ is also bounded uniformly for q (Gasser and Müller (1984)). Therefore, for $\kappa = 1, \dots, \nu$, the derivative $x_j^{(\kappa)}(t)$ is estimated by

$$\widehat{x}_j^{(\kappa)}(t) = \frac{1}{h_j^{\kappa+1}} \sum_{i=1}^{n_j} \int_{s_{i-1}}^{s_i} K_{\kappa,q}\left(\frac{t-u}{h_j}\right) du \cdot y_j(t_{ji}), \quad j = 1, 2, \dots, d. \quad (8)$$

Gasser and Müller (1984) and Gasser et al. (1985) have discussed the existence of such kernel functions $K(\cdot)$ and $K_{\nu,q}(\cdot)$, and have shown that if the sequence $\{s_i\}$ satisfies $\max_{i=1, \dots, n_j} |s_i - s_{i-1} - n_j^{-1}| = O(n_j^{-\delta})$ for some $\delta > 1$, then $\int_0^1 \|\widehat{\mathbf{x}}^{(\nu)}(t) - \mathbf{f}_0(\mathbf{x}(t), \mathbf{x}^{(1)}(t), \dots, \mathbf{x}^{(\nu-1)}(t))\|_2^2 dt = O_P(n^{-2(k-\nu)/(2k+1)})$, where $n = \min\{n_1, \dots, n_d\}$.

3.2 Stage 2: Deep Neural Network Estimator

In Stage 2, we use a multilayer feedforward neural network to approximate the unknown ground-truth $\mathbf{f}_0(\cdot)$. We start off by introducing the definitions of Hölder smoothness and compositional functions.

Definition 1. A function $g : \mathbb{R}^{r_0} \rightarrow \mathbb{R}$ is said to be (β, C) -Hölder smooth for some positive constants β and C , if for every $\gamma = (\gamma_1, \dots, \gamma_{r_0})^\top \in \mathbb{N}^{r_0}$ the following two conditions hold: letting $\kappa = \sum_{i=1}^{r_0} \gamma_i$,

$$\sup_{\mathbf{z} \in \mathbb{R}^{r_0}} \left| \frac{\partial^\kappa g}{\partial z_1^{\gamma_1} \dots \partial z_{r_0}^{\gamma_{r_0}}}(\mathbf{z}) \right| \leq C, \quad \text{if } \kappa \leq \lfloor \beta \rfloor,$$

and

$$\left| \frac{\partial^\kappa g}{\partial z_1^{\gamma_1} \dots \partial z_{r_0}^{\gamma_{r_0}}}(\mathbf{z}) - \frac{\partial^\kappa g}{\partial z_1^{\gamma_1} \dots \partial z_{r_0}^{\gamma_{r_0}}}(\tilde{\mathbf{z}}) \right| \leq C \|\mathbf{z} - \tilde{\mathbf{z}}\|_2^{\beta - \lfloor \beta \rfloor}, \quad \text{if } \kappa = \lfloor \beta \rfloor,$$

for $\mathbf{z}, \tilde{\mathbf{z}} \in \mathbb{R}^{r_0}$.

For convenience, we say g is (∞, C) -Hölder smooth if g is (β, C) -Hölder smooth for all $\beta > 0$. Hölder smoothness is commonly assumed for estimating regression functions nonparametrically in the literature (see, for instance, Stone (1985) and Ferraty and Vieu (2006)).

Definition 2. A function $f : \mathbb{R}^{r_0} \rightarrow \mathbb{R}$ is said to have a compositional structure with parameters $(L_*, \mathbf{r}, \tilde{\mathbf{r}}, \boldsymbol{\beta}, \mathbf{a}, \mathbf{b}, \mathbf{C})$ for $L_* \in \mathbb{Z}_+$, $\mathbf{r} = (r_0, \dots, r_{L_*+1})^\top \in \mathbb{Z}_+^{L_*+2}$ with $r_{L_*+1} = 1$, $\tilde{\mathbf{r}} = (\tilde{r}_0, \dots, \tilde{r}_{L_*})^\top \in \mathbb{Z}_+^{L_*+1}$, $\boldsymbol{\beta} = (\beta_0, \dots, \beta_{L_*})^\top \in \mathbb{R}_+^{L_*+1}$, $\mathbf{a} = (a_0, \dots, a_{L_*+1})^\top$, $\mathbf{b} = (b_0, \dots, b_{L_*+1})^\top \in \mathbb{R}^{L_*+2}$, and $\mathbf{C} = (C_0, \dots, C_{L_*})^\top \in \mathbb{R}_+^{L_*+1}$, if

$$f(\mathbf{z}) = \mathbf{g}_{L_*} \circ \dots \circ \mathbf{g}_1 \circ \mathbf{g}_0(\mathbf{z}), \quad \mathbf{z} \in [a_0, b_0]^{r_0},$$

where for $i = 0, 1, \dots, L_*$, $\mathbf{g}_i = (g_{i,1}, \dots, g_{i,r_{i+1}})^\top : [a_i, b_i]^{r_i} \rightarrow [a_{i+1}, b_{i+1}]^{r_{i+1}}$ for some $|a_i|, |b_i| \leq C_i$, and the functions $g_{i,j} : [a_i, b_i]^{\tilde{r}_i} \rightarrow [a_{i+1}, b_{i+1}]$ are (β_i, C_i) -Hölder smooth only relying on \tilde{r}_i variables, with $\tilde{r}_i \leq r_i$.

This definition is well connected with the structure of deep neural network (see Definition 4), where each composition can be viewed as a hidden layer in a neural network. In practice, people tend to use dropout to avoid overfitting such that only a few nodes are “active”. Thus, it is natural to assume that each component of \mathbf{g}_i only relies on \tilde{r}_i variables. Without loss of generality, we can always assume $C_i > 1$, $i = 0, \dots, L_*$. Denote by $\mathcal{CS}(L_*, \mathbf{r}, \tilde{\mathbf{r}}, \boldsymbol{\beta}, \mathbf{a}, \mathbf{b}, \mathbf{C})$ the class of compositional functions defined above. By definition, any function in $\mathcal{CS}(L_*, \mathbf{r}, \tilde{\mathbf{r}}, \boldsymbol{\beta}, \mathbf{a}, \mathbf{b}, \mathbf{C})$ is composed of $L_* + 1$ layers, and in the i -th layer, $i = 0, \dots, L_*$, there are only \tilde{r}_i “active” variables. This implicitly assumes a sparsity structure in each layer, which avoids the curse of dimensionality. Functions in each layer $g_{i,j} : [a_i, b_i]^{\tilde{r}_i} \rightarrow [a_{i+1}, b_{i+1}]$ are (β_i, C_i) -Hölder smooth and it is not difficult to verify that the composed function f is also Hölder smooth. It is pointed out by, for instance, Schmidt-Hieber (2020) that a compositional function can be approximated by a neural network with any order of

accuracy. Due to their popularity, compositional functions have been adopted by, among many others, Bauer and Kohler (2019), Schmidt-Hieber (2020), Liu et al. (2020), Kohler and Langer (2021), Wang et al. (2021), and Liu et al. (2022) to study nonparametric regression problems.

It is well known that the optimal convergence rate of a (β, C) -Hölder smooth regression function defined on \mathbb{R}^p is $n^{-\frac{2\beta}{2\beta+p}}$. When p is large, this rate suffers from the curse of dimensionality. However, for any d -dimensional function $\mathbf{f} = (f_1, \dots, f_d)^\top$ with each component f_j belonging to $\mathcal{CS}(L_*, \mathbf{r}, \tilde{\mathbf{r}}, \boldsymbol{\beta}, \mathbf{a}, \mathbf{b}, \mathbf{C})$, the “intrinsic” dimension of \mathbf{f} that actually determines the rate convergence should be less than r_0 owing to the sparsity of \mathbf{f} . Moreover, from the definition of $\mathcal{CS}(L_*, \mathbf{r}, \tilde{\mathbf{r}}, \boldsymbol{\beta}, \mathbf{a}, \mathbf{b}, \mathbf{C})$, each component of \mathbf{f} , f_j , is made up of Hölder smooth functions with the level of smoothness varying from layer to layer, and we use the concept the intrinsic smoothness to characterize the overall smoothness of f_j . Next, we introduce the definitions of the intrinsic smoothness and intrinsic dimension of the compositional functions.

Definition 3. For $f \in \mathcal{CS}(L_*, \mathbf{r}, \tilde{\mathbf{r}}, \boldsymbol{\beta}, \mathbf{a}, \mathbf{b}, \mathbf{C})$, the intrinsic smoothness and intrinsic dimension of f are defined as:

$$\beta^* = \beta_{i^*}^* \quad \text{and} \quad r^* = \tilde{r}_{i^*},$$

respectively, where $\beta_i^* = \beta_i \prod_{s=i+1}^{L_*} (\beta_s \wedge 1)$ for $i = 0, \dots, L_*$, and $i^* = \operatorname{argmin}_{0 \leq i \leq L_*} \beta_i^* / \tilde{r}_i$, with the convention $\prod_{s=L_*+1}^{L_*} (\beta_s \wedge 1) = 1$.

It is worth noting that the order of Hölder smoothness of a function f is less than its intrinsic smoothness. Throughout the paper, we assume the ground-truth $f_{0,j} \in \mathcal{CS}(L_*, \mathbf{r}, \tilde{\mathbf{r}}, \boldsymbol{\beta}, \mathbf{a}, \mathbf{b}, \mathbf{C})$, $j = 1, \dots, d$. This assumption is not restrictive, as the compositional structure covers a wide collection of functions. Here are some examples.

Example 1. (Homogeneous Linear ODE system) Consider the following dynamical system

$$\frac{d^\nu}{dt^\nu} \begin{bmatrix} x_1(t) \\ \vdots \\ x_d(t) \end{bmatrix} = \begin{bmatrix} a_{1,1} & \dots & a_{1,\nu d} \\ \vdots & \ddots & \vdots \\ a_{d,1} & \dots & a_{d,\nu d} \end{bmatrix} \begin{bmatrix} x_1(t) \\ \vdots \\ x_d^{(\nu-1)}(t) \end{bmatrix}.$$

Each component $x_j^{(\nu)}$ has a compositional structure with $L_* = 0$, $\mathbf{r} = (\nu d, 1)^\top$, $\tilde{\mathbf{r}} = \nu d$, and $\boldsymbol{\beta} = \infty$. Therefore, $\beta^* = \infty$ and $r^* = \nu d$.

The next example presents a more general case than Example 1.

Example 2. (Additive Model) Define $x_i^{(\nu)} = g_i(\sum_{j=1}^d \sum_{k=0}^{\nu-1} f_{j,k}(x_j^{(k)}))$, where $g_i(\cdot)$ is (β_g, C_g) -Hölder smooth and $f_{j,k}(\cdot)$ is (β_f, C_f) -Hölder smooth. By definition, $x_i^{(\nu)}$ can be written as a composition of three functions $x_i^{(\nu)} = h_2 \circ h_1 \circ h_0$, with $h_0(x_1, \dots, x_d^{(\nu-1)}) = (f_{1,0}(x_1), \dots, f_{d,\nu-1}(x_d^{(\nu-1)}))$,

$h_1(x_1, \dots, x_{\nu d}) = \sum_{i=1}^{\nu d} x_i$, and $h_2(x) = g_i(x)$. Here $L_* = 2, \mathbf{r} = (\nu d, \nu d, 1, 1), \tilde{\mathbf{r}} = (1, \nu d, 1), \boldsymbol{\beta} = (\beta_h, \infty, \beta_g), \beta^* = \min(\beta_h, \beta_g)$, and $r^* = 1$.

The intuition behind Definition 2 comes from the structure of feedforward neural network. We next introduce the ReLU feedforward neural network that is widely used in the deep learning literature. For $\mathbf{v} = (v_1, \dots, v_r)^\top \in \mathbb{R}^r$, define the shifted activation function $\sigma_{\mathbf{v}}(\mathbf{x}) = (\sigma(x_1 - v_1), \dots, \sigma(x_r - v_r))^\top$, where $\sigma(s) := \max\{0, s\}$ and $\mathbf{x} = (x_1, \dots, x_r)^\top \in \mathbb{R}^r$.

Definition 4. A ReLU feedforward neural network $\mathbf{f}(\mathbf{x}; W, v)$ is defined as

$$\mathbf{f}(\mathbf{x}; W, v) := W_L \sigma_{\mathbf{v}_L} \dots W_1 \sigma_{\mathbf{v}_1} W_0 \mathbf{x}, \quad \mathbf{x} \in \mathbb{R}^{p_0}, \quad (9)$$

where $W_l \in \mathbb{R}^{p_{l+1} \times p_l}, 0 \leq l \leq L$, are the weight matrices, $\mathbf{v}_l \in \mathbb{R}^{p_l}, 1 \leq l \leq L$, are referred to as biases, and p_0, p_1, \dots, p_{L+1} are positive integers.

The ReLU feedforward neural network is parameterized by $(W_j)_{j=0, \dots, L}$ and $(\mathbf{v}_j)_{j=1, \dots, L}$, where L determines the number of hidden layers. The width vector $\mathbf{p} = (p_0, \dots, p_{L+1})$ specifies the number of units in each layer, i.e., the width of the network. Clearly, a feedforward neural network belongs to $\mathcal{CS}(L_*, \mathbf{r}, \tilde{\mathbf{r}}, \boldsymbol{\beta}, \mathbf{a}, \mathbf{b}, \mathbf{C})$, with the i -th hidden layer viewed as \mathbf{g}_i .

In this paper, we consider two subclasses of ReLU feedforward neural networks:

$$\mathcal{F}_1(L, \mathbf{p}) := \{\mathbf{f}(\mathbf{x}; W, v) \text{ of form (9)} : \max_{j=0, \dots, L} \|W_j\|_\infty + |\mathbf{v}_j|_\infty \leq 1\} \quad (10)$$

where \mathbf{v}_0 is a vector of zeros, and

$$\mathcal{F}_2(L, \mathbf{p}, \tau, F) := \{\mathbf{f}(\mathbf{x}; W, v) \in \mathcal{F}_1(L, \mathbf{p}) : \sum_{j=0}^L (\|W_j\|_0 + |\mathbf{v}_j|_0) \leq \tau, \|\mathbf{f}\|_\infty \leq F\}. \quad (11)$$

The subclass (10) comprises the fully connected networks with bounded parameters, and it is not empty in that we can always rescale the weights by dividing all the weights and the biases by their maximum. In practice, people tend to use dropout as a regularization technique to prevent overfitting, i.e., randomly setting parts of neurons to zero. So it is reasonable to consider a sparse neural network as specified in (11). The two subclasses of neural networks are also considered in Schmidt-Hieber (2020) and Wang et al. (2021) which use i.i.d. data and functional data, respectively, to estimate regression function nonparametrically. In practical applications, achieving precise control over the exact number of inactive nodes in a neural network can be challenging. To address this, we adopt an alternative approach by introducing an L_1 penalty during the optimization process. This penalty effectively regulates the number of active nodes

within each layer, allowing us to attain a desirable level of sparsity in the network. This strategy provides a more practical and flexible means of controlling network complexity and achieving optimal performance. Similar approaches are used in the literature, such as those presented in Ma et al. (2019); Wang et al. (2021); Lemhadri et al. (2021).

Next, we present the estimator of the unknown ground-truth $\mathbf{f}_0(\cdot)$ in (1) via a sparsely connected deep neural network. Let $\widehat{\mathbf{x}}(t) = (\widehat{x}_1(t), \dots, \widehat{x}_d(t))^\top$ and $\widehat{\mathbf{x}}^{(\nu)}(t) = (\widehat{x}_1^{(\nu)}(t), \dots, \widehat{x}_d^{(\nu)}(t))^\top$ the kernel estimators of $\mathbf{x}(t)$ and $\mathbf{x}^{(\nu)}(t)$ obtained from Stage 1, where $\widehat{x}_j(t)$ and $\widehat{x}_j^{(\nu)}(t)$ are respectively given in (6) and (8). The idea is to search for a member in $\mathcal{F}_2(L, \mathbf{p}, \tau, F)$ that well approximates $\mathbf{f}_0(\mathbf{x}(t), \mathbf{x}^{(1)}(t), \dots, \mathbf{x}^{(\nu-1)}(t))$. Specifically, the “best” estimator of $\mathbf{f}_0(\mathbf{x}(t), \dots, \mathbf{x}^{(\nu-1)}(t))$, or equivalently $\mathbf{x}^{(\nu)}(t)$, is obtained by minimizing

$$\int_0^1 \|\widehat{\mathbf{x}}^{(\nu)}(t) - \mathbf{f}(\widehat{\mathbf{x}}(t), \widehat{\mathbf{x}}^{(1)}(t), \dots, \widehat{\mathbf{x}}^{(\nu-1)}(t); W, v)\|_2^2 dt \quad (12)$$

over all $\mathbf{f}(\mathbf{z}; W, v) \in \mathcal{F}_2(L, \mathbf{p}, \tau, F)$ with $\mathbf{p} = (r_0, p_1, \dots, p_L, d)$ and $\mathbf{z} \in \mathbb{R}^{r_0}$. The resulting estimator is denoted by $\widehat{\mathbf{f}}(\mathbf{z}; \widehat{W}, \widehat{v})$. The entire two-stage estimation procedure is summarized in Algorithm 1. Its validity is justified by the following theorem that establishes the consistency of $\widehat{\mathbf{f}}(\mathbf{z}; \widehat{W}, \widehat{v})$ as an estimator of $\mathbf{f}_0(\mathbf{x}(t), \dots, \mathbf{x}^{(\nu-1)}(t))$ and its convergence rate.

Theorem 1. *Suppose the true functions $f_{0,j} \in \mathcal{CS}(L_*, \mathbf{r}, \tilde{\mathbf{r}}, \boldsymbol{\beta}, \mathbf{a}, \mathbf{b}, C)$ with the intrinsic smoothness and intrinsic dimension β^* and r^* , respectively, $j = 1, \dots, d$. Consider the subclass $\mathcal{F}_2(L, \mathbf{p}, \tau, F)$. Let $\eta = \max_{i=0, \dots, L_*} (r_{i+1}(\tilde{r}_i + \lceil \beta_i \rceil))$ and $N = \min_{i=1, \dots, L+1} p_i$. Assume that there exist some constants \tilde{C}_i , $i = 0, \dots, L^*$, only depending on \mathbf{C}, \mathbf{a} , and \mathbf{b} such that $N \geq 6\eta \max_{i=0, \dots, L_*} (\beta_i + 1)^{\tilde{r}_i} \vee (\tilde{C}_i + 1)e^{\tilde{r}_i}$, $\tau \lesssim LN$, and $F \geq \max_{i=0, \dots, L_*} (C_i, 1)$. Then we have*

$$\begin{aligned} \int_0^1 \|\widehat{\mathbf{f}}(\mathbf{x}(t), \dots, \mathbf{x}^{(\nu-1)}(t); \widehat{W}, \widehat{v}) - \mathbf{f}_0(\mathbf{x}(t), \dots, \mathbf{x}^{(\nu-1)}(t))\|_2^2 dt &= O_P(\varsigma_n), \\ \int_0^1 \|\widehat{\mathbf{f}}(\widehat{\mathbf{x}}(t), \dots, \widehat{\mathbf{x}}^{(\nu-1)}(t); \widehat{W}, \widehat{v}) - \mathbf{f}_0(\mathbf{x}(t), \dots, \mathbf{x}^{(\nu-1)}(t))\|_2^2 dt &= O_P(\varsigma_n), \end{aligned}$$

where $\varsigma_n = (1 + N^L)n^{-2(k-\nu)/(2k+1)} + (N2^{-L})^2 \prod_{i=1}^{L_*} \beta_i \wedge 1 + N^{-\frac{2\beta^*}{r^*}}$.

To simplify the notation, we have assumed in Theorem 1 that the intrinsic smoothness and intrinsic dimension of the components of \mathbf{f}_0 are all the same. Theorem 1 is still valid if this assumption is relaxed, by setting β^* and r^* to the lower bound of the intrinsic smoothness and the upper bound of the intrinsic dimension, respectively, over the components of \mathbf{f}_0 .

The convergence rate in Theorem 1 contains three parts: the first part $n^{-2(k-\nu)/(2k+1)}$ is the approximation error due to the kernel method; the second part $N^L n^{-2(k-\nu)/(2k+1)}$ corresponds to

Algorithm 1 Training $\widehat{\mathbf{f}}(\mathbf{z}; \widehat{W}, \widehat{v})$

Input: observed values $\{\mathbf{y}_1, \dots, \mathbf{y}_d\}$, feed-forward neural network $\mathbf{f}(\mathbf{z}; W, v) \in \mathcal{F}_2(L, \mathbf{p}, \tau, F)$, number of epochs E , and learning rate α

for each component j , $j = 1, \dots, d$, **do**

Estimate $x_j(t)$ and its higher order derivative $x_j^{(\kappa)}(t)$, $\kappa = 1, \dots, \nu$, through (6) and (8), respectively: $\widehat{x}_j(t) = \frac{1}{h_j} \sum_{i=1}^{n_j} \int_{s_{i-1}}^{s_i} K(\frac{t-u}{h_j}) du \cdot y_j(t_{ji})$ and $\widehat{x}_j^{(\kappa)}(t) = \frac{1}{h_j^{\kappa+1}} \sum_{i=1}^{n_j} \int_{s_{i-1}}^{s_i} K_{\kappa,q}(\frac{t-u}{h_j}) du \cdot y_j(t_{ji})$

where the tuning parameter can be determined by cross validation

end for

Use $(\widehat{\mathbf{x}}(t), \widehat{\mathbf{x}}^{(1)}(t), \dots, \widehat{\mathbf{x}}^{(\nu-1)}(t))$ as the input to fit $\widehat{\mathbf{x}}^{(\nu)}(t)$ through minimizing the loss function defined as $\ell(W, v) = \int_0^1 \|\widehat{\mathbf{x}}^{(\nu)}(t) - \mathbf{f}(\widehat{\mathbf{x}}(t), \widehat{\mathbf{x}}^{(1)}(t), \dots, \widehat{\mathbf{x}}^{(\nu-1)}(t); W, v)\|_2^2 dt$

Initialize W, v

for $e \in \{1, \dots, E\}$ **do**

Compute gradient of the loss $\ell(W, v)$ with respect to the parameters

$(W, v), \nabla_W \ell(W, v), \nabla_v \ell(W, v)$ using back-propagation

Update $W \leftarrow W - \alpha \nabla_W \ell(W, v), v \leftarrow v - \alpha \nabla_v \ell(W, v)$

end for

Output: $\widehat{\mathbf{f}}(\mathbf{z}; \widehat{W}, \widehat{v})$

perturbation error of neural network; the last part $(N2^{-L})^2 \prod_{l=1}^{L^*} \beta_l \wedge 1 + N^{-\frac{2\beta^*}{r^*}}$ is associated with the approximation of $\mathcal{F}_2(L, \mathbf{p}, \tau, F)$ to \mathbf{f}_0 . Note that ς_n is free of the input dimension d which helps us get around the curse of dimensionality. The consistency of $\widehat{\mathbf{f}}(\mathbf{z}; \widehat{W}, \widehat{v})$ is guaranteed, if the tuning parameters are suitably selected, for instance, $L \asymp (\log n)^{1/2}$ and $N \asymp e^{(\log n)^{1/4}}$, since the latter implies $\varsigma_n \rightarrow 0$ as $n \rightarrow \infty$.

3.3 Variable Selection

Owing to the sparseness assumption in $\mathcal{CS}(L_*, \mathbf{r}, \tilde{\mathbf{r}}, \boldsymbol{\beta}, \mathbf{a}, \mathbf{b}, \mathbf{C})$, it is natural to assume $f_{0,j}$ is also sparsely represented. In many cases, the right-hand side of (1) or (4) involves only a few input variables, rather than the entire set $(x_1(t), \dots, x_d(t), x_1^{(1)}(t), \dots, x_d^{(1)}(t), \dots, x_1^{(\nu-1)}(t), \dots, x_d^{(\nu-1)}(t))$. Moreover, the set of relevant input variables may well vary from component to component; that is, the active input variables that relate to $x_j^{(\nu)}(t)$ are not necessarily the same as those to $x_{j'}^{(\nu)}(t)$, $j' \neq j$. However, the estimator $\widehat{\mathbf{f}}(\mathbf{z}; \widehat{W}, \widehat{v})$ obtained by minimizing (12) cannot select the relevant subset from the collection of the input variables. Lemhadri et al. (2021) propose a new feature/variable selection framework for neural networks by adding a penalized input-to-output residual layer and selecting the active features only if the corresponding weights are nonzero. To facilitate variable selection in (4), inspired by Lemhadri et al. (2021), we modify the ReLU feedforward neural network considered in Stage 2 and introduce a new class of neural network $f_{\text{vs}}(\mathbf{z}; \boldsymbol{\theta}, W, v)$ for each component, which is defined as

$$f_{\text{vs}}(\mathbf{z}; \boldsymbol{\theta}, W, v) = \boldsymbol{\theta}^\top \mathbf{z} + f(\mathbf{z}; W, v) \quad (13)$$

where $f(\mathbf{z}; W, v) \in \mathcal{F}_2(L, \mathbf{p}, \tau, F)$ with $\mathbf{p} = (r_0, p_1, \dots, p_L, 1)$ and $\boldsymbol{\theta}, \mathbf{z} \in \mathbb{R}^{r_0}$. The difference between $f_{\text{vs}}(\mathbf{z}; \boldsymbol{\theta}, W, v)$ and the standard feed-forward neural network is the inclusion of the residual layer $\boldsymbol{\theta}^\top \mathbf{z}$ which makes it considerably easier in tackling the vanishing gradient problem.

Assume that $f_{0,j}$ involves only a subset of the input variables $(x_1(t), \dots, x_d(t), x_1^{(1)}(t), \dots, x_d^{(1)}(t), \dots, x_1^{(\nu-1)}(t), \dots, x_d^{(\nu-1)}(t))$. We first estimate $x_1(t), \dots, x_d(t)$ and their derivatives via the kernel method outlined in Section 3.1, and then solve the following optimization problem in order to obtain the estimator of $f_{0,j}$: $\widehat{f}_{\text{vs},j}(\mathbf{z}; \widehat{\boldsymbol{\theta}}, \widehat{W}, \widehat{v}) = \widehat{\boldsymbol{\theta}}^\top \mathbf{z} + f(\mathbf{z}; \widehat{W}, \widehat{v})$, with

$$\begin{aligned} (\widehat{\boldsymbol{\theta}}, \widehat{W}, \widehat{v}) = \operatorname{argmin} \int_0^1 \left\| \widehat{x}_j^{(\nu)}(t) - f_{\text{vs}}(\widehat{\mathbf{x}}(t), \widehat{\mathbf{x}}^{(1)}(t), \dots, \widehat{\mathbf{x}}^{(\nu-1)}(t); \boldsymbol{\theta}, W, v) \right\|_2^2 dt + \lambda \|\boldsymbol{\theta}\|_1, \\ \text{subject to } \|W_{0,i}\|_\infty \leq M|\theta_i|, i = 1, \dots, r_0, \end{aligned} \quad (14)$$

In (14), θ_i is the i -component of $\boldsymbol{\theta} \in \mathbb{R}^{r_0}$ and $W_{0,i}$ contains the weights for the i -th input variable in the first hidden layer. There are two tuning parameters in the objective function: λ and M , which

penalize the linear and nonlinear components simultaneously. The constraint $\|W_{0,i}\|_\infty \leq M|\theta_i|$ plays a vital role, in that M leverages the effect of the i -th input variable, thereby capturing the non-linearity in the data. When $M = 0$, the neural network part in $f_{\text{vs}}(\mathbf{z}; \boldsymbol{\theta}, W, v)$ vanishes and $f_{\text{vs}}(\mathbf{z}; \boldsymbol{\theta}, W, v) = \boldsymbol{\theta}^\top \mathbf{z}$, and thus (14) degenerates to standard LASSO. When $M \rightarrow \infty$, we get a feed-forward network with an ℓ_1 penalty on the residual layer. Following the optimization procedure outlined in Lemhadri et al. (2021), we optimize the objective function (14) using hierarchical proximal gradient descent. Hierarchical proximal operator is a widely used algorithm for solving composite optimization problems where the objective function can be decomposed into a sum of several components, each with its own convex structure. For further insights, refer to Chambolle and Pock (2011); Bauschke and Combettes (2017). It is worth mentioning that without domain knowledge, it is difficult to determine the value of M . In practical implementation, we use cross validation to select M , a common practice in machine learning algorithms. The detailed pseudocode is summarized in Algorithm 2.

3.4 Computational Complexity

In this section, we assess the computational cost of the proposed procedure. We break down the time complexity into two main components: the kernel estimator in Stage 1 and the deep neural network estimator in Stage 2. It is noteworthy that both stages encompass integral computations and can leverage various numerical algorithms with a time complexity of $O(n)$, such as Simpson's method and the Newton-Cotes method. For a comprehensive review of these numerical algorithms, refer to Burden et al. (2015). For the first stage, it is evident that the time complexity for each time-point, denoted as $\hat{x}_j(t)$ and $\hat{x}_j^{(\kappa)}(t)$ where $j = 1, \dots, d$ and $\kappa = 1, \dots, \nu$, amounts to $O(n_j^2)$. Let $\tilde{n} = \max\{n_1, \dots, n_d\}$. In terms of training $\hat{\mathbf{f}}(\mathbf{z}; \widehat{W}, \widehat{v})$ in second stage, the time complexity per training sample hinges on the number of layers L , the neuron count in each layer represented by $\mathbf{p} = (p_0, \dots, p_{L+1})$, and the number of epochs E . Both the feed-forward and backpropagation phases involve matrix multiplications. Given that the weight matrix W_l in the l th layer has dimension $p_{l+1} \times p_l$, the time complexity within each layer is $O(p_{l+1}p_l)$. Since the overall structure comprises L layers, the time complexity can be approximated as $O(E \sum_{l=1}^L p_{l+1}p_l)$. The training $\hat{f}_{\text{vs},j}(\mathbf{z}; \widehat{\boldsymbol{\theta}}, \widehat{W}, \widehat{v})$ involves the hierarchical proximal gradient descent. Notably, since only the first layer's weight matrix is penalized, and in accordance with Bauschke and Combettes (2017); Lemhadri et al. (2021), the computational complexity of hierarchical proximal gradient descent is controlled by $O(p_0p_1 \log(p_0p_1))$, which is negligible in comparison to the computation required for updating other parameters. Thus, the computational complexity of training $\hat{f}_{\text{vs},j}(\mathbf{z}; \widehat{\boldsymbol{\theta}}, \widehat{W}, \widehat{v})$ is

Algorithm 2 Training $\widehat{f}_{\text{vs},j}(\mathbf{z}; \widehat{\boldsymbol{\theta}}, \widehat{W}, \widehat{v})$

Input: observed values $\{\mathbf{y}_1, \dots, \mathbf{y}_d\}$, $f(\mathbf{z}; W, v) \in \mathcal{F}_2(L, \mathbf{p}, \tau, F)$, number of epochs E , learning rate α , hyper-parameter M , and path multiplier ϵ

for each component j , $j = 1, \dots, d$, **do**

Estimate $x_j(t)$ and its higher order derivative $x_j^{(\kappa)}(t)$, $\kappa = 1, \dots, \nu$ through (6) and (8), respectively: $\widehat{x}_j(t) = \frac{1}{h_j} \sum_{i=1}^{n_j} \int_{s_{i-1}}^{s_i} K(\frac{t-u}{h_j}) du \cdot y_j(t_{ji})$ and $\widehat{x}_j^{(\kappa)}(t) = \frac{1}{h_j^{\kappa+1}} \sum_{i=1}^{n_j} \int_{s_{i-1}}^{s_i} K_{\kappa,q}(\frac{t-u}{h_j}) du \cdot y_j(t_{ji})$

where the tuning parameter can be determined by cross validation

end for

Use $(\widehat{\mathbf{x}}(t), \widehat{\mathbf{x}}^{(1)}(t), \dots, \widehat{\mathbf{x}}^{(\nu-1)}(t))$ as the input to fit $\widehat{x}_j^{(\nu)}(t)$ through minimizing the loss function defined as $\ell = \ell(\boldsymbol{\theta}, W, v) = \int_0^1 \left\| \widehat{x}_j^{(\nu)}(t) - f_{\text{vs},j}(\widehat{\mathbf{x}}(t), \widehat{\mathbf{x}}^{(1)}(t), \dots, \widehat{\mathbf{x}}^{(\nu-1)}(t); \boldsymbol{\theta}, W, v) \right\|_2^2 dt + \lambda \|\boldsymbol{\theta}\|_1$,

Initialize $\boldsymbol{\theta}, W, v$, $\lambda = \epsilon$, $k = r_0$

while $k > 0$ **do**

Update $\lambda \leftarrow (1 + \epsilon)\lambda$

for $e \in \{1, \dots, E\}$ **do**

Compute gradients $\nabla_{\boldsymbol{\theta}} \ell, \nabla_W \ell, \nabla_v \ell$ using back-propagation

Update $\boldsymbol{\theta} \leftarrow \boldsymbol{\theta} - \alpha \nabla_{\boldsymbol{\theta}} \ell$, $W \leftarrow W - \alpha \nabla_W \ell$, $v \leftarrow v - \alpha \nabla_v \ell$

Update $(\boldsymbol{\theta}, W_0) \leftarrow \text{Hier-Prox}(\boldsymbol{\theta}, W_0, \alpha \lambda, M)$, where Hier-Prox is provided in Algorithm 3

in the Appendix.

end for

Update k to be the number of non-zero elements of $\boldsymbol{\theta}$

end while

Output: $\widehat{f}_{\text{vs},j}(\mathbf{z}; \widehat{\boldsymbol{\theta}}, \widehat{W}, \widehat{v})$

the same as training $\widehat{\mathbf{f}}(\mathbf{z}; \widehat{W}, \widehat{v})$.

4 Numerical Experiments

In this section, we carry out simulation studies to assess the finite sample performance of the proposed two-stage estimation procedure and variable selection algorithm for two different designs of ODE systems. In both designs, we use the same network architecture with length $L = 3$ and width $N = 30$. The tuning parameters in the first stage of estimation procedure are selected by cross validation. The dropout probability is set to 0.2 to avoid overfitting. Summary statistics from each simulation setting are calculated based on 100 independent simulation runs.

4.1 Simulation Study 1

In the first simulation study (i.e., Design 1), we consider a second order nonlinear ODE system:

$$\begin{aligned} x_1^{(2)}(t) &= 2 \frac{x_1^{(1)}(t)}{x_3^{(1)}(t)} + 4x_4^{(1)}(t) - x_3(t)x_4(t), \\ x_2^{(2)}(t) &= -x_4^{(1)}(t), \quad x_3^{(2)}(t) = 2, \\ x_4^{(2)}(t) &= x_2^{(1)}(t), \quad x_5^{(2)}(t) = x_5(t), \\ x_6^{(2)}(t) &= -x_5^2(t)x_6(t) + x_6^{(1)}(t), \\ x_7^{(2)}(t) &= x_7^{(1)}(t)x_2^{(1)}(t) - x_2(t)x_7(t), \\ x_8^{(2)}(t) &= -(x_8^{(1)}(t))^2. \end{aligned}$$

The noisy data are computed via $y_{ji} = x_j(t_i) + \epsilon_{ji}$, for $i = 1, \dots, n$ and $j = 1, \dots, 8$, with $t_i = i/n$ and ϵ_{ji} sampled independently from $N(0, \sigma^2)$. We consider three noise levels: $\sigma = 0.2, 0.5, 0.8$, and the sample size n is chosen from $n \in \{100, 200, 500\}$. We treat the first 80% of the data, i.e., $\{y_{ji}, i = 1, 2, \dots, 0.8n\}$ as the training set, and the remaining are put aside as the test set.

In this experiment, we aim to evaluate the performance of the procedure described in Sections

3.1 and 3.2. To this end, the following metrics are employed:

$$\begin{aligned}
M_1 &= \int_{0.8}^1 \left\| \widehat{\mathbf{f}}(\mathbf{x}(t), \mathbf{x}^{(1)}(t), \dots, \mathbf{x}^{(\nu-1)}(t)) - \mathbf{f}_0(\mathbf{x}(t), \dots, \mathbf{x}^{(\nu-1)}(t)) \right\|_2 dt, \\
M_2 &= \int_{0.8}^1 \left\| \widehat{\mathbf{f}}(\widehat{\mathbf{x}}(t), \widehat{\mathbf{x}}^{(1)}(t), \dots, \widehat{\mathbf{x}}^{(\nu-1)}(t)) - \mathbf{f}_0(\mathbf{x}(t), \dots, \mathbf{x}^{(\nu-1)}(t)) \right\|_2 dt, \\
M_3 &= \max_{j=1, \dots, d} \int_{0.8}^1 \left| \widehat{f}_j(\mathbf{x}(t), \mathbf{x}^{(1)}(t), \dots, \mathbf{x}^{(\nu-1)}(t)) - f_{0,j}(\mathbf{x}(t), \dots, \mathbf{x}^{(\nu-1)}(t)) \right| dt, \\
M_4 &= \max_{j=1, \dots, d} \int_{0.8}^1 \left| \widehat{f}_j(\widehat{\mathbf{x}}(t), \widehat{\mathbf{x}}^{(1)}(t), \dots, \widehat{\mathbf{x}}^{(\nu-1)}(t)) - f_{0,j}(\mathbf{x}(t), \dots, \mathbf{x}^{(\nu-1)}(t)) \right| dt.
\end{aligned}$$

Metrics M_1 and M_3 measure the differences between the target and the second-stage deep neural network estimator in the L_2 norm and in the max norm, respectively, while M_2 and M_4 gauge the overall performance of the proposed two-stage estimator via these two norms. All the metrics are computed using the test data.

Table 1 reports the averaged values of the four metrics and their standard deviations (in parentheses) over 100 replications for different combinations of noise level and sample size. As expected, the deviations measured by M_2 (M_4) are greater than those by M_1 (M_3) unanimously. Our results also show that the accuracy of the estimator diminishes the noise-to-signal ratio increases. Nevertheless, a larger sample size always yields a smaller deviation across all cases, which is in line with the theoretical results.

4.2 Simulation Study 2

In the second simulation (Design 2), we suppose that the true data generating process is governed by the following homogeneous first order linear ODE system:

$$\mathbf{x}^{(1)}(t) = A\mathbf{x}(t) + \mathbf{b}, \quad 0 \leq t \leq 1,$$

where A is a $d \times d$ sparse matrix and \mathbf{b} is a d -dimensional vector referred to as the initial value. Elements of \mathbf{b} are sampled from the uniform distribution $U(0, 1)$. We further define a set $J = \{j_1, j_2, j_3, j_4, j_5\}$, where $j_k, k = 1, \dots, 5$, are randomly sampled from $\{1, \dots, d\}$ without replacement. The coefficient matrix $A = (a_{ij})_{d \times d}$ is sparse and its elements are defined in the following way: for $i = 1, \dots, d$, if $j \in J$, then a_{ij} is sampled from $U(0, 1)$; otherwise, $a_{ij} = 0$. In other words, each row of A has five non-zero values that are sampled from the uniform distribution. It is easy to verify that for $j = 1, \dots, d$, $f_{0,j} \in \mathcal{CS}(L_*, \mathbf{r}, \tilde{\mathbf{r}}, \boldsymbol{\beta}, \mathbf{a}, \mathbf{b}, C)$ with $L_* = 0$, $\mathbf{r} = (d, 1)^\top$, $\tilde{\mathbf{r}} = 5$, $\boldsymbol{\beta} = \infty, \beta^* = \infty$, and $r^* = 5$. For simplicity, we set $n_1 = n_2 = \dots = n_d = n$. The ‘‘observed’’ data are generated from $y_{ji} = x_j(t_i) + \epsilon_{ji}$, $i = 1, \dots, n, j = 1, \dots, d$, where $t_i = i/n$ and ϵ_{ji} are

sampled from $N(0, 1)$. The sample size n and dimension d are chosen to be $n = 100, 200, 500$ and $d = 10, 100, 1000$. The train-test split is the same as the first simulation.

The objective of this study is twofold. Firstly, we want to check how the dimension d impacts the accuracy of the two-stage estimation procedure for the linear system, and to evaluate the variable selection algorithm. Secondly, we would like to compare our method with GRADE by Chen et al. (2017) which utilizes a nonparametric approach to estimate high-dimensional additive ordinary differential equations and achieve variable selection.

For each $j = 1, \dots, d$, we use the method described in Section 3.3 to find $\hat{f}_{vs,j}(z)$. Let $\hat{\mathbf{f}} = (\hat{f}_{vs,1}, \dots, \hat{f}_{vs,d})^\top$. Similar to Section 4.1, we use M_1, M_2, M_3 , and M_4 to assess the estimation errors. In order to evaluate the performance of variable selection, we consider the following two metrics:

- MinSize = the minimum number of selected variables to includes all true variables
- ProbAll = the success rate that the selected five variables are all true variables

These two metrics are widely used in feature selection literature (see, for instance, Zhong and Zhu (2015) and Li et al. (2012)). By definition, MinSize is expected to be at least five; and the closer to five, the better the procedure. The metric ProbAll measures the sensitivity (true positive) rate of the method in detecting the true variables. A higher value of ProbAll is desirable, as this indicates there is a higher chance that the algorithm will pick all the true variables.

The simulation results that summarize the estimation errors are reported in Table 2, while the variable selection results are in Table 3. Table 2 indicates that (i) although increasing dimension exerts an adverse impact on the accuracy of the estimator, a large sample size can easily offset the impact; (ii) our method performs better than GRADE across all the values of n and d under consideration. As for the variable selection accuracy, we observe from Table 3 that our method yields a much smaller minimum selection size than GRADE, albeit greater than five, and that the probability of selecting all the true variables is higher when using our method than that of GRADE. The simulation results in both tables demonstrate the effectiveness of our method, especially when dimension d is large.

5 Real Data Analysis

In this section, we illustrate our proposed method by the COVID-19 infection cases. The data are downloaded from *New York Times*. (2021) <https://github.com/nytimes/covid-19-data>. This dataset consists of daily new COVID-19 cases reported in individual states across the United

Table 1: Simulation results of Design 1 for the proposed method. The table reports the averaged values of the four metrics and their standard deviations (in parentheses) over 100 replications for different combinations of noise level σ and sample size n .

		$\sigma = 0.2$	$\sigma = 0.5$	$\sigma = 0.8$
Metric M_1	$n = 100$	0.050 (0.007)	0.081 (0.008)	0.142 (0.017)
	$n = 200$	0.044 (0.005)	0.051 (0.006)	0.085 (0.011)
	$n = 500$	0.034 (0.003)	0.041 (0.004)	0.049 (0.005)
Metric M_2	$n = 100$	0.061 (0.011)	0.122 (0.016)	0.188 (0.021)
	$n = 200$	0.052 (0.006)	0.092 (0.009)	0.126 (0.014)
	$n = 500$	0.049 (0.004)	0.079 (0.006)	0.097 (0.008)
Metric M_3	$n = 100$	0.224 (0.024)	0.274 (0.034)	0.476 (0.051)
	$n = 200$	0.196 (0.017)	0.211 (0.023)	0.285 (0.029)
	$n = 500$	0.181 (0.012)	0.201 (0.015)	0.212 (0.018)
Metric M_4	$n = 100$	0.226 (0.037)	0.375 (0.041)	0.614 (0.071)
	$n = 200$	0.204 (0.028)	0.302 (0.033)	0.410 (0.047)
	$n = 500$	0.197 (0.017)	0.255 (0.021)	0.302 (0.028)

States from 03/23/2020 to 05/07/2021, with a total of 411 observations for each state. As an example, the orange curves in the four panels of Figure 1 depict the number of the recorded daily new cases in California, Texas, New York, and Florida, respectively.

Here, we would like to use a system of ODEs to characterize the rate of changes of new cases over the 50 states *simultaneously*. Specifically, we consider a 50-dimensional second order ODE system, as in (1) with $\mathbf{x}(t) = (x_1(t), \dots, x_{50}(t))^T$ representing the number of COVID-19 cases at time t . With the daily new cases, we first calculate the daily cases accumulated since 03/23/2020 for each state, i.e., y_{ji} in (3) for $i = 1, 2, \dots, 411$, $j = 1, 2, \dots, 50$. We then use the proposed estimation approach to estimate $\mathbf{x}(t)$, its derivatives, and the function \mathbf{f}_0 . Specifically, we use a neural network with length $L = 3$ and width $N = 50$ with dropout probability equals to 0.2. The filtered daily new cases $\hat{\mathbf{x}}(t)$ are shown as blue curves in Figure 1 for the four selected states, while the deep neural network estimator $\hat{\mathbf{f}}_0$ is shown in green. The results demonstrate the effectiveness and foreseeability of our method: when the estimated growth rate reaches the highest value, the daily new cases will peak roughly one month later.

To further illustrate the strength of our approach, we compare the proposed method with the traditional nonparametric estimation of the derivative of the regression function that estimates

Table 2: Simulation results of Design 2 for the proposed method and GRADE. The table reports the averaged values of the four metrics and their standard deviations (in parentheses) over 100 replications for different combinations of dimension d and sample size n .

		Methods	$d = 10$	$d = 100$	$d = 1000$
Metric M_1	$n = 100$	Our Method	0.331 (0.034)	0.387 (0.042)	0.756 (0.081)
		GRADE	0.448 (0.053)	0.554 (0.062)	1.144 (0.131)
	$n = 200$	Our Method	0.198 (0.019)	0.206 (0.022)	0.241 (0.021)
		GRADE	0.309 (0.031)	0.352 (0.047)	0.383 (0.055)
	$n = 500$	Our Method	0.103 (0.005)	0.111 (0.005)	0.126 (0.009)
		GRADE	0.169 (0.010)	0.182 (0.017)	0.199 (0.025)
Metric M_2	$n = 100$	Our Method	0.498 (0.052)	0.559 (0.076)	1.004 (0.144)
		GRADE	0.732 (0.087)	0.876 (0.101)	1.423 (0.199)
	$n = 200$	Our Method	0.239 (0.022)	0.258 (0.031)	0.301 (0.034)
		GRADE	0.357 (0.038)	0.383 (0.067)	0.418 (0.072)
	$n = 500$	Our Method	0.134 (0.013)	0.140 (0.011)	0.177 (0.025)
		GRADE	0.202 (0.017)	0.254 (0.031)	0.309 (0.039)
Metric M_3	$n = 100$	Our Method	1.01 (0.108)	2.364 (0.184)	8.406 (0.633)
		GRADE	1.763 (0.205)	3.758 (0.445)	12.214 (1.913)
	$n = 200$	Our Method	0.682 (0.058)	1.086 (0.103)	2.008 (0.124)
		GRADE	1.148 (0.133)	1.823 (0.243)	3.456 (0.536)
	$n = 500$	Our Method	0.343 (0.044)	0.701 (0.088)	1.019 (0.111)
		GRADE	0.507 (0.114)	1.068 (0.148)	1.516 (0.299)
Metric M_4	$n = 100$	Our Method	1.348 (0.138)	2.920 (0.380)	9.150 (0.510)
		GRADE	1.997 (0.227)	4.010 (0.494)	14.317 (2.366)
	$n = 200$	Our Method	0.821 (0.122)	1.271 (0.149)	2.273 (0.273)
		GRADE	1.225 (0.159)	1.994 (0.273)	3.933 (0.630)
	$n = 500$	Our Method	0.394 (0.032)	0.759 (0.053)	1.109 (0.099)
		GRADE	0.639 (0.133)	1.123 (0.172)	1.727 (0.334)

Table 3: Simulation results of Design 2 for the proposed method and GRADE. The table reports the averaged values of the two metrics that assess the variable selection accuracy and their standard deviations (in parentheses) over 100 replications for different combinations of dimension d and sample size n .

		Methods	$d = 10$	$d = 100$	$d = 1000$
MinSize	$n = 100$	Our Method	5.78 (1.06)	6.37 (1.17)	7.26 (1.26)
		GRADE	6.99 (1.23)	8.09 (1.32)	9.49 (1.48)
	$n = 200$	Our Method	5.46 (0.94)	5.98 (1.13)	6.84 (1.21)
		GRADE	6.73 (1.19)	7.59 (1.28)	9.11 (1.43)
	$n = 500$	Our Method	5.32 (0.89)	5.69 (1.09)	6.36 (1.16)
		GRADE	6.19 (1.02)	7.27 (1.22)	8.38 (1.38)
		Methods	$d = 10$	$d = 100$	$d = 1000$
ProbAll	$n = 100$	Our Method	0.92	0.82	0.67
		GRADE	0.83	0.71	0.49
	$n = 200$	Our Method	0.94	0.86	0.72
		GRADE	0.85	0.75	0.53
	$n = 500$	Our Method	0.96	0.92	0.79
		GRADE	0.89	0.81	0.55

the growth rate of each state separately. The top two panels in Figure 2 show the growth rates that are estimated separately for three states in the western (Utah, Nevada, and Idaho) and northeastern (Connecticut, Rhode Island, and Massachusetts) U.S., respectively. The growth rates estimated using our method are depicted in the bottom two panels. To facilitate the comparison, we standardize the growth rate by dividing it by its respective population size. It is apparent that there is a discrepancy between the two estimates, and our estimates are more consistent with what is expected: geographically adjacent states should have strong interactions, thereby sharing similar growth rates. This further shows the superiority of our method, in that it effectively incorporates the interactive processes among the neighboring states.

To better understand the interactions of these states, we apply our variable selection method described in Section 3.3 to the data from Massachusetts. The top three states that are associated with Massachusetts are: New York State, Rhode Island, and Connecticut.

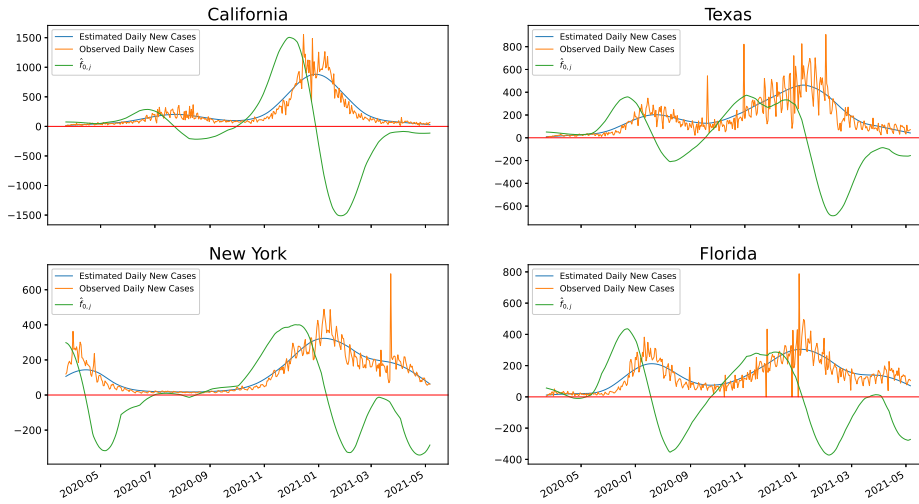


Figure 1: The orange curve depicts the observed daily new COVID cases from 03/23/2020 to 05/07/2021 in California, Texas, New York State, and Florida, respectively. The blue curve is the estimated daily new cases, while the green one is the estimated growth rates.

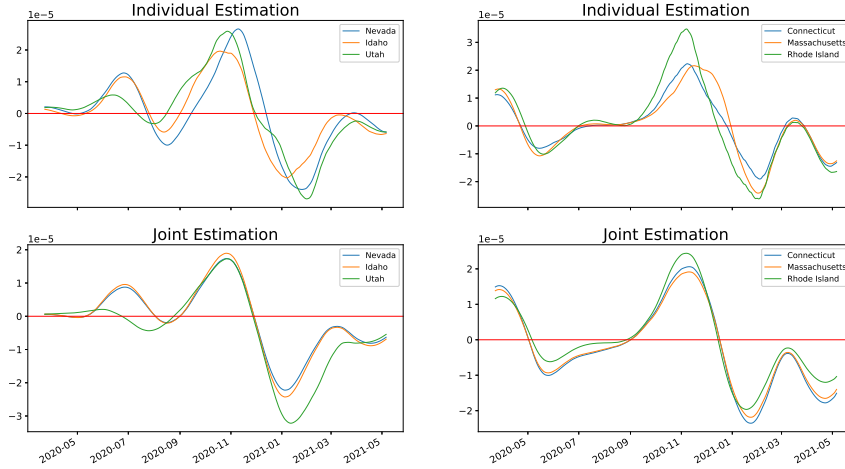


Figure 2: A comparison between individual estimation (top two panels) and joint estimation (bottom two panels). Left two panels: western states. Right two panels: northeastern states.

6 Conclusion

In this study, we have introduced a novel nonparametric approach for estimating large-scale ordinary differential equation (ODE) systems from noisy data, particularly in cases involving intricate and nonlinear relationships among input variables. Our methodology addresses the challenge of accurately recovering ODE structures, even in the presence of complex underlying functions.

We have demonstrated the consistent capability of our proposed method to recover ODE structures, even when the true functional relationships are complex. The adoption of the state-of-the-art framework developed by Lemhadri et al. (2021) for neural network feature selection enhances our approach’s applicability, allowing it to excel even in scenarios with nonlinear ODE systems. Rigorous simulation studies and a real data analysis have substantiated the validity and effectiveness of our methods.

However, our work is not without its limitations. One notable challenge lies in the substantial computational resources demanded by training deep neural networks, particularly in the context of high-dimensional systems. Finding strategies to balance computational efficiency with accuracy will be a crucial avenue for future research. Moreover, our current formulation assumes a specific noise distribution in the data. A more robust approach should be explored to accommodate a broader range of noise distributions, thereby enhancing the method’s robustness and practicality.

Furthermore, while our approach excels in estimating complex functions, extracting meaning-

ful biological, physical, or chemical insights from the estimated parameters remains a challenge. To enhance the interpretability of the obtained ODE structures, future research could focus on developing post-processing techniques that facilitate the extraction of valuable domain-specific knowledge from the estimated models.

Looking forward, exciting opportunities lie in the integration of our approach with causal inference techniques. This integration could shed light on the causal relationships inherent in ODE systems, paving the way for more nuanced and informed insights. Additionally, incorporating domain knowledge and prior information through appropriate regularization terms could enhance the accuracy and interpretability of the estimated ODE models.

In conclusion, our work contributes to advancing the field of ODE system estimation through a flexible and accurate methodology. While acknowledging its limitations, we have identified various directions for future research that hold promise in enhancing the methodology’s robustness, efficiency, interpretability, and integration with other powerful analytical techniques. These avenues offer a rich landscape for researchers to explore and continue pushing the boundaries of accurate and interpretable ODE modeling.

References

- Bahdanau, D., K. Cho, and Y. Bengio (2014). Neural machine translation by jointly learning to align and translate. *arXiv preprint arXiv:1409.0473*.
- Bauer, B. and M. Kohler (2019, 08). On deep learning as a remedy for the curse of dimensionality in nonparametric regression. *Ann. Statist.* 47(4), 2261–2285.
- Bauschke, H. H. and P. L. Combettes (2017). *Convex Analysis and Monotone Operator Theory in Hilbert Spaces* (2nd ed.). Springer Publishing Company, Incorporated.
- Benson, M. (1979). Parameter fitting in dynamic models. *Ecological Modelling* 6(2), 97 – 115.
- Bhaumik, P. and S. Ghosal (2015). Bayesian two-step estimation in differential equation models. *Electron. J. Statist.* 9(2), 3124–3154.
- Biegler, L. T., J. J. Damiano, and G. E. Blau (1986). Nonlinear parameter estimation: A case study comparison. *AIChE Journal* 32(1), 29–45.
- Burden, R. L., J. D. Faires, and A. M. Burden (2015). *Numerical analysis*. Cengage learning.
- Chambolle, A. and T. Pock (2011). A first-order primal-dual algorithm for convex problems with applications to imaging. *Journal of mathematical imaging and vision* 40, 120–145.
- Champion, K., B. Lusch, J. N. Kutz, and S. L. Brunton (2019). Data-driven discovery of coordinates and governing equations. *Proceedings of the National Academy of Sciences* 116(45), 22445–22451.
- Chen, R. T. Q., Y. Rubanova, J. Bettencourt, and D. K. Duvenaud (2018). Neural ordinary differential equations. In S. Bengio, H. Wallach, H. Larochelle, K. Grauman, N. Cesa-Bianchi, and R. Garnett (Eds.), *Advances in Neural Information Processing Systems*, Volume 31, pp. 6571–6583. Curran Associates, Inc.
- Chen, S., A. Shojaie, and D. M. Witten (2017). Network reconstruction from high-dimensional ordinary differential equations. *Journal of the American Statistical Association* 112(520), 1697–1707. PMID: 29618851.
- Elbrächter, D., D. Perekrestenko, P. Grohs, and H. Bölcskei (2021). Deep neural network approximation theory. *IEEE Transactions on Information Theory* 67(5), 2581–2623.

- Farrell, M. H., T. Liang, and S. Misra (2021). Deep neural networks for estimation and inference. *Econometrica* 89(1), 181–213.
- Ferraty, F. and P. Vieu (2006). *Nonparametric functional data analysis: theory and practice*. Springer Science & Business Media.
- Gasser, T. and H.-G. Müller (1984). Estimating regression functions and their derivatives by the kernel method. *Scandinavian Journal of Statistics* 11(3), 171–185.
- Gasser, T., H.-G. Müller, and V. Mammitzsch (1985). Kernels for nonparametric curve estimation. *Journal of the Royal Statistical Society. Series B (Methodological)* 47(2), 238–252.
- Hall, P. and Y. Ma (2014). Quick and easy one-step parameter estimation in differential equations. *Journal of the Royal Statistical Society: Series B (Statistical Methodology)* 76(4), 735–748.
- Hammer, B. (2000). On the approximation capability of recurrent neural networks. *Neurocomputing* 31(1), 107 – 123.
- Hartford, J., G. Lewis, K. Leyton-Brown, and M. Taddy (2017). Deep iv: A flexible approach for counterfactual prediction. In *International Conference on Machine Learning*, pp. 1414–1423. PMLR.
- He, K., X. Zhang, S. Ren, and J. Sun (2016). Deep residual learning for image recognition. In *2016 IEEE Conference on Computer Vision and Pattern Recognition (CVPR)*, pp. 770–778.
- Henderson, J. and G. Michailidis (2014, 04). Network reconstruction using nonparametric additive ode models. *PLOS ONE* 9(4), 1–15.
- Henderson, K. and M. Loreau (2019). An ecological theory of changing human population dynamics. *People and Nature* 1(1), 31–43.
- Kobyzev, I., S. Prince, and M. Brubaker (2020). Normalizing flows: An introduction and review of current methods. *IEEE Transactions on Pattern Analysis and Machine Intelligence*, 1–1.
- Kohler, M. and S. Langer (2021). On the rate of convergence of fully connected deep neural network regression estimates. *The Annals of Statistics* 49(4), 2231 – 2249.
- Lemhadri, I., F. Ruan, L. Abraham, and R. Tibshirani (2021). Lassonet: A neural network with feature sparsity. *Journal of Machine Learning Research* 22(127), 1–29.

- Li, K. (2022). Variable selection for nonlinear cox regression model via deep learning. *arXiv preprint arXiv:2211.09287*.
- Li, K., F. Wang, L. Yang, and R. Liu (2023). Deep feature screening: Feature selection for ultra high-dimensional data via deep neural networks. *Neurocomputing* 538, 126186.
- Li, K., J. Zhu, A. R. Ives, V. C. Radeloff, and F. Wang (2023). Semiparametric regression for spatial data via deep learning. *arXiv preprint arXiv:2301.03747*.
- Li, Q., T. Lin, and Z. Shen (2019). Deep learning via dynamical systems: An approximation perspective. *arXiv preprint arXiv:1912.10382*.
- Li, R., W. Zhong, and L. Zhu (2012). Feature screening via distance correlation learning. *Journal of the American Statistical Association* 107(499), 1129–1139.
- Li, Z., J. Han, W. E, and Q. Li (2020). On the curse of memory in recurrent neural networks: Approximation and optimization analysis. *arXiv preprint arXiv:2009.07799*.
- Liang, H. and H. Wu (2008). Parameter estimation for differential equation models using a framework of measurement error in regression models. *Journal of the American Statistical Association* 103(484), 1570–1583. PMID: 19956350.
- Liu, R., B. Boukai, and Z. Shang (2022). Optimal nonparametric inference via deep neural network. *Journal of Mathematical Analysis and Applications* 505(2), 125561.
- Liu, R., Z. Shang, and G. Cheng (2020). On deep instrumental variables estimate. *arXiv preprint arXiv:2004.14954*.
- Lu, J., Z. Shen, H. Yang, and S. Zhang (2021). Deep network approximation for smooth functions. *SIAM Journal on Mathematical Analysis* 53(5), 5465–5506.
- Lu, T., H. Liang, H. Li, and H. Wu (2011). High-dimensional odes coupled with mixed-effects modeling techniques for dynamic gene regulatory network identification. *Journal of the American Statistical Association* 106(496), 1242–1258. PMID: 23204614.
- Lusch, B., J. Kutz, and S. Brunton (2018). Deep learning for universal linear embeddings of nonlinear dynamics. *Nat Commun* 9, 4950.
- Ma, R., J. Miao, L. Niu, and P. Zhang (2019). Transformed l1 regularization for learning sparse deep neural networks. *Neural Networks* 119, 286–298.

- Min, S., B. Lee, and S. Yoon (2017). Deep learning in bioinformatics. *Briefings in bioinformatics* 18(5), 851–869.
- Paul, D., J. Peng, and P. Burman (2016). Nonparametric estimation of dynamics of monotone trajectories. *The Annals of Statistics* 44(6), 2401–2432.
- Priestley, M. B. and M. Chao (1972). Non-parametric function fitting. *Journal of the Royal Statistical Society: Series B (Methodological)* 34(3), 385–392.
- Schmidt-Hieber, J. (2020, 08). Nonparametric regression using deep neural networks with relu activation function. *Ann. Statist.* 48(4), 1875–1897.
- Stone, C. J. (1985). Additive regression and other nonparametric models. *The annals of Statistics*, 689–705.
- Sun, M., D. Zeng, and Y. Wang (2020, 09). Modelling temporal biomarkers with semiparametric nonlinear dynamical systems. *Biometrika* 108(1), 199–214.
- Talwar, S. and N. Namachchivaya Sri (1992, December). Control of chaotic systems: Application to the lorenz equations. In *Nonlinear Vibrations*, American Society of Mechanical Engineers, Design Engineering Division (Publication) DE, pp. 47–58. Publ by ASME. Winter Annual Meeting of the American Society of Mechanical Engineers ; Conference date: 08-11-1992 Through 13-11-1992.
- Wang, S., G. Cao, Z. Shang, and for the Alzheimer’s Disease Neuroimaging Initiative (2021). Estimation of the mean function of functional data via deep neural networks. *Stat* 10(1), e393.
- Weinan, E. (2017). A proposal on machine learning via dynamical systems. *Communications in Mathematics and Statistics* 5(1), 1–11.
- Wu, L., X. Qiu, Y. X. Yuan, and H. Wu (2019). Parameter estimation and variable selection for big systems of linear ordinary differential equations: A matrix-based approach. *Journal of the American Statistical Association* 114(526), 657–667.
- Zhang, S., L. Yao, A. Sun, and Y. Tay (2019). Deep learning based recommender system: A survey and new perspectives. *ACM computing surveys (CSUR)* 52(1), 1–38.
- Zhang, X., J. Cao, and R. J. Carroll (2015). On the selection of ordinary differential equation models with application to predator-prey dynamical models. *Biometrics* 71(1), 131–138.

Zhong, W. and L. Zhu (2015). An iterative approach to distance correlation-based sure independence screening. *Journal of Statistical Computation and Simulation* 85(11), 2331–2345.

A Proof of Theorem 1

The proof of Theorem 1 requires some preliminary lemmas.

Lemma 1. *For any $f : \mathbb{R}^{r_0} \rightarrow \mathbb{R} \in \mathcal{CS}(L_*, \mathbf{r}, \tilde{\mathbf{r}}, \beta, \mathbf{a}, \mathbf{b}, \mathbf{C})$, integer $m > 0$ and $N \geq \max_{i=0, \dots, L_*} (\beta_i + 1)^{\tilde{r}_i} \vee (\tilde{C}_i + 1)e^{\tilde{r}_i}$, there exists a neural network*

$$f_* \in \mathcal{F}_2(L, (r_0, 6\eta N, \dots, 6\eta N, 1), \sum_{i=0}^{L_*} r_{i+1}(\tau_i + 4), \infty),$$

where

$$\begin{aligned} \tilde{C}_i &= \sum_{i=0}^i C_i \frac{b_i - a_i}{b_{i+1} - a_{i+1}}, i = 0, \dots, L_* - 1, \\ \tilde{C}_{L_*} &= \sum_{i=0}^{L_*} C_i \frac{b_i - a_i}{b_{i+1} - a_{i+1}} + b_{L_*} - a_{L_*} \\ L &= 3L_* + \sum_{i=0}^{L_*} L_i, \\ L_i &= 8 + (m + 5)(1 + \lceil \log_2(\tilde{r}_i \vee \beta_i) \rceil), \\ \tau_i &\leq 141(\tilde{r}_i + \beta_i + 1)^{3+\tilde{r}_i} N(m + 6), \\ \eta &= \max_{i=0, \dots, L_*} (r_{i+1}(\tilde{r}_i + \lceil \beta_i \rceil)), \end{aligned}$$

such that

$$\|f_* - f\|_\infty \leq C_{L_*} \prod_{l=0}^{L_*-1} (2C_l)^{\beta_{l+1}} \sum_{i=0}^{L_*} \left((2\tilde{C}_i + 1)(1 + \tilde{r}_i^2 + \beta_i^2) 6^{\tilde{r}_i} N 2^{-m} + \tilde{C}_i 3^{\beta_i} N^{-\frac{\beta_i}{\tilde{r}_i}} \right)^{\prod_{l=i+1}^{L_*} \beta_l \wedge 1}.$$

Proof. Suppose

$$f(\mathbf{z}) = \mathbf{g}_{L_*} \circ \dots \circ \mathbf{g}_1 \circ \mathbf{g}_0(\mathbf{z}), \quad \text{for } \mathbf{z} \in [a_0, b_0]^{r_0}$$

where $\mathbf{g}_i = (g_{i,1}, \dots, g_{i,r_{i+1}})^\top : [a_i, b_i]^{r_i} \rightarrow [a_{i+1}, b_{i+1}]^{r_{i+1}}$ for some $|a_i|, |b_i| \leq C_i$ and the functions $g_{i,j} : [a_i, b_i]^{\tilde{r}_i} \rightarrow [a_{i+1}, b_{i+1}]$ are (β_i, C_i) -Hölder smooth. For $i = 0, \dots, L_* - 1$, the domain and range of \mathbf{g}_i are $[a_i, b_i]^{r_i}$ and $[a_{i+1}, b_{i+1}]^{r_{i+1}}$. In the first step, we will rewrite f as the composition of functions $\mathbf{h}_i := (h_{i,1}, \dots, h_{i,r_{i+1}})^\top$ whose domain and range are $[0, 1]^{r_i}$ and $[0, 1]^{r_{i+1}}$ by linear transformation. That is, we define

$$\begin{aligned} \mathbf{h}_i(\mathbf{z}) &:= \frac{\mathbf{g}_i((b_i - a_i)\mathbf{z} - a_{i+1})}{b_{i+1} - a_{i+1}}, \quad \text{for } \mathbf{z} \in [0, 1]^{r_i}, i = 0, \dots, L_* - 1 \\ \mathbf{h}_{L_*}(\mathbf{z}) &:= \mathbf{g}_{L_*}((b_{L_*} - a_{L_*})\mathbf{z} + a_{L_*}), \quad \text{for } \mathbf{z} \in [0, 1]^{r_{L_*}}. \end{aligned}$$

And the following equality holds

$$f(\mathbf{z}) = \mathbf{g}_{L_*} \circ \dots \circ \mathbf{g}_1 \circ \mathbf{g}_0(\mathbf{z}) = \mathbf{h}_{L_*} \circ \dots \circ \mathbf{h}_1 \circ \mathbf{h}_0\left(\frac{\mathbf{z} - \mathbf{a}_0}{\mathbf{b}_0 - \mathbf{a}_0}\right), \quad \text{for } \mathbf{z} \in [\mathbf{a}_0, \mathbf{b}_0]^{r_0}$$

Since $g_{i,j} : [a_i, b_i]^{\tilde{r}_i} \rightarrow [a_{i+1}, b_{i+1}]$ are all (β_i, C_i) -Hölder smooth, it follows that $h_{i,j} : [0, 1]^{\tilde{r}_i} \rightarrow [0, 1]$ are all (β_i, \tilde{C}_i) -Hölder smooth, where \tilde{C}_i is a constant only depends on $\mathbf{a}, \mathbf{b}, \mathbf{C}$, i.e., $\tilde{C}_i = \sum_{i=0}^i C_i \frac{b_i - a_i}{b_{i+1} - a_{i+1}}, i = 0, \dots, L_* - 1, \tilde{C}_{L_*} = \sum_{i=0}^{L_*} C_i \frac{b_i - a_i}{b_{i+1} - a_{i+1}} + b_{L_*} - a_{L_*}$.

By Theorem 5 in Schmidt-Hieber (2020), for any integer $m \geq 1$ and $N \geq \max_{i=0, \dots, L_*} (\beta_i + 1)^{\tilde{r}_i} \vee (\tilde{C}_i + 1)e^{\tilde{r}_i}$, there exist a network

$$\tilde{h}_{i,j} \in \mathcal{F}_2(L_i, (\tilde{r}_i, 6(\tilde{r}_i + \lceil \beta_i \rceil)N, \dots, 6(\tilde{r}_i + \lceil \beta_i \rceil)N, 1), \tau_i, \infty),$$

with $L_i = 8 + (m + 5)(1 + \lceil \log_2(\tilde{r}_i \vee \beta_i) \rceil)$, $\tau_i \leq 141(\tilde{r}_i + \beta_i + 1)^{3+\tilde{r}_i} N(m + 6)$, such that

$$\|\tilde{h}_{i,j} - h_{i,j}\|_\infty \leq (2\tilde{C}_i + 1)(1 + \tilde{r}_i^2 + \beta_i^2)6^{\tilde{r}_i} N 2^{-m} + \tilde{C}_i 3^{\beta_i} N^{-\frac{\beta_i}{\tilde{r}_i}}.$$

Note that the value of $\tilde{h}_{i,j}$ is $(-\infty, \infty)$, so we define $h_{i,j}^* := \sigma(-\sigma(-\tilde{h}_{i,j} + 1) + 1)$ by add two more layers $\sigma(1 - x)$ to restrict $h_{i,j}^*$ into the interval $[0, 1]$. This introduces two more layers and four more parameters and the by the fact that $h_{i,j} \in [0, 1]$, we have $h_{i,j}^* \in \mathcal{F}_2(L_i + 2, (\tilde{r}_i, 6(\tilde{r}_i + \lceil \beta_i \rceil)N, \dots, 6(\tilde{r}_i + \lceil \beta_i \rceil)N, 1), \tau_i + 4, \infty)$ and

$$\|h_{i,j}^* - h_{i,j}\|_\infty \leq \|\tilde{h}_{i,j} - h_{i,j}\|_\infty \leq (2\tilde{C}_i + 1)(1 + \tilde{r}_i^2 + \beta_i^2)6^{\tilde{r}_i} N 2^{-m} + \tilde{C}_i 3^{\beta_i} N^{-\frac{\beta_i}{\tilde{r}_i}}.$$

We further parallelize all $(h_{i,j}^*)_{j=1, \dots, r_{i+1}}$ together, then we get $\mathbf{h}_i^* := (h_{i,1}^*, \dots, h_{i,r_{i+1}}^*)^\top \in \mathcal{F}_2(L_i + 2, (r_i, 6r_{i+1}(\tilde{r}_i + \lceil \beta_i \rceil)N, \dots, 6r_{i+1}(\tilde{r}_i + \lceil \beta_i \rceil)N, r_{i+1}), r_{i+1}(\tau_i + 4), \infty)$. Moreover, we construct the composite network $f_* := \mathbf{h}_{L_*}^* \circ \dots \circ \mathbf{h}_1^* \circ \mathbf{h}_0^* \in \mathcal{F}_2(3L_* + \sum_{i=0}^{L_*} L_i, (r_0, 6\eta N, \dots, 6\eta N, 1), \sum_{i=0}^{L_*} r_{i+1}(\tau_i + 4), \infty)$, where $\eta = \max_{i=0, \dots, L_*} (r_{i+1}(\tilde{r}_i + \lceil \beta_i \rceil))$.

By Lemma 3 in Schmidt-Hieber (2020), we conclude the following inequality holds

$$\begin{aligned} \|f - f_*\|_\infty &= \|\mathbf{h}_{L_*} \circ \dots \circ \mathbf{h}_1 \circ \mathbf{h}_0 - \mathbf{h}_{L_*}^* \circ \dots \circ \mathbf{h}_1^* \circ \mathbf{h}_0^*\|_\infty \\ &\leq C_{L_*} \prod_{l=0}^{L_*-1} (2C_l)^{\beta_{l+1}} \sum_{i=0}^{L_*} \|\mathbf{h}_i - \mathbf{h}_i^*\|_\infty^{\prod_{l=i+1}^{L_*} \beta_l \wedge 1} \\ &\leq C_{L_*} \prod_{l=0}^{L_*-1} (2C_l)^{\beta_{l+1}} \sum_{i=0}^{L_*} \left((2\tilde{C}_i + 1)(1 + \tilde{r}_i^2 + \beta_i^2)6^{\tilde{r}_i} N 2^{-m} + \tilde{C}_i 3^{\beta_i} N^{-\frac{\beta_i}{\tilde{r}_i}} \right)^{\prod_{l=i+1}^{L_*} \beta_l \wedge 1} \\ &\leq C_{L_*} \prod_{l=0}^{L_*-1} (2C_l)^{\beta_{l+1}} \sum_{i=0}^{L_*} ((2\tilde{C}_i + 1)(1 + \tilde{r}_i^2 + \beta_i^2)6^{\tilde{r}_i} N 2^{-m})^{\prod_{l=i+1}^{L_*} \beta_l \wedge 1} + \\ &\quad C_{L_*} \prod_{l=0}^{L_*-1} (2C_l)^{\beta_{l+1}} \sum_{i=0}^{L_*} (\tilde{C}_i 3^{\beta_i} N^{-\frac{\beta_i}{\tilde{r}_i}})^{\prod_{l=i+1}^{L_*} \beta_l \wedge 1} \end{aligned}$$

□

Proof of Theorem 1:

Without loss of generality, we only consider the case when n is sufficiently large. Let

$$\hat{\mathbf{f}}(\mathbf{z}, \hat{W}, \hat{v}) := \operatorname{argmin}_{\mathbf{f} \in \mathcal{F}_2(L, \mathbf{p}, \tau, F)} \int_0^1 \left\| \hat{\mathbf{x}}^{(\nu)}(t) - \mathbf{f}(\hat{\mathbf{x}}(t), \hat{\mathbf{x}}^{(1)}(t), \dots, \hat{\mathbf{x}}^{(\nu-1)}(t), W, v) \right\|_2^2 dt, \mathbf{z} \in \mathbb{R}^{r_0},$$

$$\tilde{\mathbf{f}}(\mathbf{z}, \tilde{W}, \tilde{v}) := \operatorname{argmin}_{\mathbf{f} \in \mathcal{F}_2(L, \mathbf{p}, \tau, F)} \int_0^1 \left\| \mathbf{x}^{(\nu)}(t) - \mathbf{f}(\mathbf{x}(t), \mathbf{x}^{(1)}(t), \dots, \mathbf{x}^{(\nu-1)}(t), W, v) \right\|_2^2 dt, \mathbf{z} \in \mathbb{R}^{r_0},$$

$$\check{\mathbf{f}}(\mathbf{z}, \check{W}, \check{v}) := \operatorname{argmin}_{\mathbf{f} \in \mathcal{F}_2(L, \mathbf{p}, \tau, F)} \sum_{i=1}^n \left\| \mathbf{x}^{(\nu)}(t_i) - \mathbf{f}(\mathbf{x}(t_i), \mathbf{x}^{(1)}(t_i), \dots, \mathbf{x}^{(\nu-1)}(t_i), W, v) \right\|_2^2, \mathbf{z} \in \mathbb{R}^{r_0}.$$

For simplicity, we use $\hat{\mathbf{f}}, \tilde{\mathbf{f}}, \check{\mathbf{f}}$ to represent $\hat{\mathbf{f}}(\mathbf{z}, \hat{W}, \hat{v}), \tilde{\mathbf{f}}(\mathbf{z}, \tilde{W}, \tilde{v})$ and $\check{\mathbf{f}}(\mathbf{z}, \check{W}, \check{v})$.

By the definition of $\hat{\mathbf{f}}$ and $\tilde{\mathbf{f}}$ we can obtain

$$\begin{aligned} \int_0^1 \left\| \hat{\mathbf{f}}(\hat{\mathbf{x}}(t), \hat{\mathbf{x}}^{(1)}(t), \dots, \hat{\mathbf{x}}^{(\nu-1)}(t)) - \hat{\mathbf{x}}^{(\nu)}(t) \right\|_2^2 dt &\leq \int_0^1 \left\| \tilde{\mathbf{f}}(\hat{\mathbf{x}}(t), \hat{\mathbf{x}}^{(1)}(t), \dots, \hat{\mathbf{x}}^{(\nu-1)}(t)) - \hat{\mathbf{x}}^{(\nu)}(t) \right\|_2^2 dt \\ \int_0^1 \left\| \tilde{\mathbf{f}}(\mathbf{x}(t), \mathbf{x}^{(1)}(t), \dots, \mathbf{x}^{(\nu-1)}(t)) - \mathbf{x}^{(\nu)}(t) \right\|_2^2 dt &\leq \int_0^1 \left\| \hat{\mathbf{f}}(\mathbf{x}(t), \mathbf{x}^{(1)}(t), \dots, \mathbf{x}^{(\nu-1)}(t)) - \mathbf{x}^{(\nu)}(t) \right\|_2^2 dt \\ \int_0^1 \left\| \tilde{\mathbf{f}}(\mathbf{x}(t), \mathbf{x}^{(1)}(t), \dots, \mathbf{x}^{(\nu-1)}(t)) - \mathbf{x}^{(\nu)}(t) \right\|_2^2 dt &\leq \int_0^1 \left\| \check{\mathbf{f}}(\mathbf{x}(t), \mathbf{x}^{(1)}(t), \dots, \mathbf{x}^{(\nu-1)}(t)) - \mathbf{x}^{(\nu)}(t) \right\|_2^2 dt \end{aligned}$$

Using the above inequalities, we can decompose the error into the following four terms:

$$\begin{aligned}
& \int_0^1 \|\hat{\mathbf{f}}(\mathbf{x}(t), \mathbf{x}^{(1)}(t), \dots, \mathbf{x}^{(\nu-1)}(t)) - \mathbf{f}_0(\mathbf{x}(t), \mathbf{x}^{(1)}(t), \dots, \mathbf{x}^{(\nu-1)}(t))\|_2^2 dt \\
& \lesssim \int_0^1 \|\hat{\mathbf{f}}(\mathbf{x}(t), \mathbf{x}^{(1)}(t), \dots, \mathbf{x}^{(\nu-1)}(t)) - \hat{\mathbf{f}}(\hat{\mathbf{x}}(t), \hat{\mathbf{x}}^{(1)}(t), \dots, \hat{\mathbf{x}}^{(\nu-1)}(t))\|_2^2 dt \\
& \quad + \int_0^1 \|\hat{\mathbf{x}}^{(\nu)}(t) - \mathbf{f}_0(\mathbf{x}(t), \mathbf{x}^{(1)}(t), \dots, \mathbf{x}^{(\nu-1)}(t))\|_2^2 dt \\
& \quad + \int_0^1 \|\hat{\mathbf{f}}(\hat{\mathbf{x}}(t), \hat{\mathbf{x}}^{(1)}(t), \dots, \hat{\mathbf{x}}^{(\nu-1)}(t)) - \hat{\mathbf{x}}^{(\nu)}(t)\|_2^2 dt \\
& \lesssim T_1 + T_2 + \int_0^1 \|\tilde{\mathbf{f}}(\hat{\mathbf{x}}(t), \hat{\mathbf{x}}^{(1)}(t), \dots, \hat{\mathbf{x}}^{(\nu-1)}(t)) - \hat{\mathbf{x}}^{(\nu)}(t)\|_2^2 dt \\
& \lesssim T_1 + T_2 \\
& \quad + \int_0^1 \|\tilde{\mathbf{f}}(\mathbf{x}(t), \mathbf{x}^{(1)}(t), \dots, \mathbf{x}^{(\nu-1)}(t)) - \tilde{\mathbf{f}}(\hat{\mathbf{x}}(t), \hat{\mathbf{x}}^{(1)}(t), \dots, \hat{\mathbf{x}}^{(\nu-1)}(t))\|_2^2 dt \\
& \quad + \int_0^1 \|\hat{\mathbf{x}}^{(\nu)}(t) - \mathbf{f}_0(\mathbf{x}(t), \mathbf{x}^{(1)}(t), \dots, \mathbf{x}^{(\nu-1)}(t))\|_2^2 dt \\
& \quad + \int_0^1 \|\tilde{\mathbf{f}}(\mathbf{x}(t), \mathbf{x}^{(1)}(t), \dots, \mathbf{x}^{(\nu-1)}(t)) - \mathbf{x}^{(\nu)}(t)\|_2^2 dt \\
& \lesssim T_1 + 2T_2 + T_3 \\
& \quad + \int_0^1 \|\check{\mathbf{f}}(\mathbf{x}(t), \mathbf{x}^{(1)}(t), \dots, \mathbf{x}^{(\nu-1)}(t)) - \mathbf{x}^{(\nu)}(t)\|_2^2 dt \\
& = T_1 + 2T_2 + T_3 + T_4,
\end{aligned}$$

where

$$\begin{aligned}
T_1 &= \int_0^1 \|\hat{\mathbf{f}}(\mathbf{x}(t), \mathbf{x}^{(1)}(t), \dots, \mathbf{x}^{(\nu-1)}(t)) - \hat{\mathbf{f}}(\hat{\mathbf{x}}(t), \hat{\mathbf{x}}^{(1)}(t), \dots, \hat{\mathbf{x}}^{(\nu-1)}(t))\|_2^2 dt, \\
T_2 &= \int_0^1 \|\hat{\mathbf{x}}^{(\nu)}(t) - \mathbf{f}_0(\mathbf{x}(t), \mathbf{x}^{(1)}(t), \dots, \mathbf{x}^{(\nu-1)}(t))\|_2^2 dt, \\
T_3 &= \int_0^1 \|\tilde{\mathbf{f}}(\mathbf{x}(t), \mathbf{x}^{(1)}(t), \dots, \mathbf{x}^{(\nu-1)}(t)) - \tilde{\mathbf{f}}(\hat{\mathbf{x}}(t), \hat{\mathbf{x}}^{(1)}(t), \dots, \hat{\mathbf{x}}^{(\nu-1)}(t))\|_2^2 dt, \\
T_4 &= \int_0^1 \|\check{\mathbf{f}}(\mathbf{x}(t), \mathbf{x}^{(1)}(t), \dots, \mathbf{x}^{(\nu-1)}(t)) - \mathbf{x}^{(\nu)}(t)\|_2^2 dt.
\end{aligned}$$

The error consists of four parts. T_1 and T_3 can be viewed as the perturbation error of neural network. T_2 is the approximation error from the kernel estimator in stage 1. The last term T_4 is the approximation error of neural network. We will analyze these four terms separately.

Suppose $x_j(t)$ is k times differentiable and there is a modified kernel $K_{\nu,q}$. Furthermore, if the sequence $\{s_i\}$ satisfies $\max_i |s_i - s_{i-1} - n^{-1}| = O(n^{-\delta})$ for some $\delta > 1$, it follows from Theorem 5

in Gasser and Müller (1984) that

$$\int_0^1 \|\widehat{\mathbf{x}}^{(\nu)}(t) - \mathbf{f}_0(\mathbf{x}(t), \mathbf{x}^{(1)}(t), \dots, \mathbf{x}^{(\nu-1)}(t))\|_2^2 dt = O_P(n^{-2(k-\nu)/(2k+1)}), \quad (15)$$

where $\widehat{\mathbf{x}}^{(\nu)}(t) = (\widehat{x}_1^{(\nu)}(t), \dots, \widehat{x}_d^{(\nu)}(t))^\top$.

For T_1 , Let $\mathbf{x} := (\mathbf{x}(t), \mathbf{x}^{(1)}(t), \dots, \mathbf{x}^{(\nu-1)}(t))$, $\widehat{\mathbf{x}} := (\widehat{\mathbf{x}}(t), \widehat{\mathbf{x}}^{(1)}(t), \dots, \widehat{\mathbf{x}}^{(\nu-1)}(t))$, and $\boldsymbol{\delta} := \widehat{\mathbf{x}} - \mathbf{x} \in \mathbb{R}^{r_0}$. As $n \rightarrow \infty$, by (15), we know $|\boldsymbol{\delta}| \lesssim (\frac{1}{n^{2(k-\nu)/(2k+1)}}, \dots, \frac{1}{n^{2(k-\nu)/(2k+1)}})$. Meanwhile, define $\widehat{\mathbf{f}}(\mathbf{x}, \hat{W}, \hat{v}) = \hat{W}_L \sigma_{\hat{v}_L} \dots \hat{W}_1 \sigma_{\hat{v}_1} \hat{W}_0 \mathbf{x}$. Let $\tau_j = \|\hat{W}_j\|_0 + |\hat{v}_j|_0$, the number of non-zero entries in the j -th layer. Since $\max(\|\hat{W}_j\|_\infty, |\hat{v}_j|_\infty) \leq 1$ and the fact $|\sigma_{\hat{v}_j}(\mathbf{x} + \boldsymbol{\delta}) - \sigma_{\hat{v}_j}(\mathbf{x})| \leq |\boldsymbol{\delta}|$, we can easily get

$$\begin{aligned} & \|\widehat{\mathbf{f}}(\mathbf{x}, \mathbf{x}^{(1)}, \dots, \mathbf{x}^{(\nu-1)}) - \widehat{\mathbf{f}}(\widehat{\mathbf{x}}, \widehat{\mathbf{x}}^{(1)}, \dots, \widehat{\mathbf{x}}^{(\nu-1)})\|_\infty^2 \\ &= \|\hat{W}_L \sigma_{\hat{v}_L} \hat{W}_{L-1} \sigma_{\hat{v}_{L-1}} \dots \sigma_{\hat{v}_0} \hat{W}_0 \mathbf{x} - \hat{W}_L \sigma_{\hat{v}_L} \hat{W}_{L-1} \sigma_{\hat{v}_{L-1}} \dots \sigma_{\hat{v}_0} \hat{W}_0 (\mathbf{x} + \boldsymbol{\delta})\|_\infty^2 \\ &\leq \tau_0 \|\hat{W}_L \sigma_{\hat{v}_L} \hat{W}_{L-1} \sigma_{\hat{v}_{L-1}} \dots \sigma_{\hat{v}_1} \hat{W}_1 \boldsymbol{\delta}\|_\infty^2 \\ &\leq \Pi_{j=0}^L \tau_j \|\boldsymbol{\delta}\|_\infty^2 \\ &\leq \left(\frac{\sum_{j=1}^L \tau_j}{L}\right)^L \|\boldsymbol{\delta}\|_\infty^2 = \left(\frac{\tau}{L}\right)^L \|\boldsymbol{\delta}\|_\infty^2 = O_P\left(\left(\frac{\tau}{L}\right)^L n^{-2(k-\nu)/(2k+1)}\right), \end{aligned}$$

which implies $T_1 = O_P\left(\left(\frac{\tau}{L}\right)^L n^{-2(k-\nu)/(2k+1)}\right)$.

For T_2 , by (15), we know $T_2 = O_P(n^{-2(k-\nu)/(2k+1)})$.

For T_3 , similar to T_1 , we can show $T_3 = O_P\left(\left(\frac{\tau}{L}\right)^L n^{-2(k-\nu)/(2k+1)}\right)$.

For T_4 , since each true functions $f_{0,j} \in \mathcal{CS}(L_*, \mathbf{r}, \tilde{\mathbf{r}}, \boldsymbol{\beta}, \mathbf{a}, \mathbf{b}, \mathbf{C})$, $j = 1, \dots, d$, let us consider the following estimation problems:

$$\begin{aligned} \tilde{f}_j &= \operatorname{argmin}_{f \in \mathcal{F}_2(L, \mathbf{p}, \tau, F)} \int_0^1 \left\| \mathbf{x}_j^{(\nu)}(t) - f(\mathbf{x}(t), \mathbf{x}^{(1)}(t), \dots, \mathbf{x}^{(\nu-1)}(t), W, v) \right\|_2^2 dt, \\ \check{f}_j &= \operatorname{argmin}_{f \in \mathcal{F}_2(L, \mathbf{p}, \tau, F)} \sum_{i=1}^n \left\| \mathbf{x}_j^{(\nu)}(t_i) - f(\mathbf{x}(t_i), \mathbf{x}^{(1)}(t_i), \dots, \mathbf{x}^{(\nu-1)}(t_i), W, v) \right\|_2^2. \end{aligned}$$

By Theorem 2 in Schmidt-Hieber (2020), we get the following inequality

$$\int_0^1 \|\tilde{f}_j - f_{0,j}\|_2^2 dt \leq \int_0^1 \|\check{f}_j - f_{0,j}\|_2^2 dt = O\left(\inf_{f \in \mathcal{F}_2(L, \mathbf{p}, \tau, F)} \|f - f_{0,j}\|_\infty^2\right). \quad (16)$$

Now we need to analyze $\inf_{f \in \mathcal{F}_2(L, \mathbf{p}, \tau, F)} \|f - f_{0,j}\|_\infty^2$. Since $f_{0,j} \in \mathcal{CS}(L_*, \mathbf{r}, \tilde{\mathbf{r}}, \boldsymbol{\beta}, \mathbf{a}, \mathbf{b}, \mathbf{C})$, $j = 1, \dots, d$, by Lemma 1, for any $m > 0$, there exists a neural network

$$f_{*,j} \in \mathcal{F}_2(L, (r_0, N, \dots, N, 1), \tau, \infty),$$

with $L \asymp m$, $N \geq 6\eta \max_{i=0,\dots,L_*} (\beta_i + 1)^{\tilde{r}_i} \vee (\tilde{C}_i + 1)e^{\tilde{r}_i}$, $\eta = \max_{i=0,\dots,L_*} (r_{i+1}(\tilde{r}_i + \lceil \beta_i \rceil))$, $\tau \lesssim mN$, such that

$$\begin{aligned} \|f_{*,j} - f_{0,j}\|_\infty &\lesssim \sum_{i=0}^{L_*} (N2^{-m}) \Pi_{l=i+1}^{L_*} \beta_l \wedge 1 + (N^{-\frac{\beta_i}{\tilde{r}_i}}) \Pi_{l=i+1}^{L_*} \beta_l \wedge 1 \\ &\lesssim \sum_{i=0}^{L_*} (N2^{-m}) \Pi_{l=i+1}^{L_*} \beta_l \wedge 1 + N^{-\frac{\beta_i^*}{\tilde{r}_i^*}} \\ &\lesssim (N2^{-m}) \Pi_{l=1}^{L_*} \beta_l \wedge 1 + N^{-\frac{\beta^*}{r^*}}, \end{aligned}$$

where β^* and r^* are the intrinsic smoothness and intrinsic dimension defined in Definition 3. This means there exists a sequence of networks $(f_n)_n$ such for all sufficiently large n , $\|f_n - f_{0,j}\|_\infty \lesssim (N2^{-m}) \Pi_{l=1}^{L_*} \beta_l \wedge 1 + N^{-\frac{\beta^*}{r^*}}$ and $f_n \in \mathcal{F}_2(L, \mathbf{p}, \tau, \infty)$. Next define $\hat{f}_j := f_n(\|f_{0,j}\|_\infty / \|f_n\|_\infty \wedge 1) \in \mathcal{F}_2(L, \mathbf{p}, \tau, F)$ and $\|\hat{f}_j - f_{0,j}\|_\infty \lesssim (N2^{-m}) \Pi_{l=1}^{L_*} \beta_l \wedge 1 + N^{-\frac{\beta^*}{r^*}}$. Then it follows that $\inf_{f \in \mathcal{F}_2(L, \mathbf{p}, \tau, F)} \|f - f_{0,j}\|_\infty \lesssim \|\hat{f}_j - f_{0,j}\|_\infty \lesssim (N2^{-m}) \Pi_{l=1}^{L_*} \beta_l \wedge 1 + N^{-\frac{\beta^*}{r^*}}$.

Since the length, minimum width, active neurons for all \hat{f}_j has the same order, and d is a fixed constant, we can synchronize the number of hidden layers for all \hat{f}_j by adding the some additional layers with identity weight matrix. After parallelizing the above d networks \hat{f}_j , we can get the joint neural network $\mathbf{f}^* \in \mathcal{F}_2(L, (r_0, N, \dots, N, d), \tau, F)$ satisfying $F \geq \max(\max_{i=0,\dots,L_*} C_i, 1)$, with $L \asymp m$, $N \geq \max_{i=0,\dots,L_*} (\beta_i + 1)^{\tilde{r}_i} \vee (\tilde{C}_i + 1)e^{\tilde{r}_i}$, $\tau \lesssim mN$, such that

$$\|\mathbf{f}^* - \mathbf{f}_0\|_\infty \lesssim (N2^{-m}) \Pi_{l=1}^{L_*} \beta_l \wedge 1 + N^{-\frac{\beta^*}{r^*}}.$$

Combine with (16), it holds that

$$T_4 = O\left((N2^{-m})^2 \Pi_{l=1}^{L_*} \beta_l \wedge 1 + N^{-\frac{2\beta^*}{r^*}}\right).$$

Combining the above we get

$$\varsigma_n = (1 + N^L)n^{-2(k-\nu)/(2k+1)} + (N2^{-L})^2 \Pi_{l=1}^{L_*} \beta_l \wedge 1 + N^{-\frac{2\beta^*}{r^*}}$$

As a consequence, by the fact that

$$\begin{aligned} &\int_0^1 \|\hat{\mathbf{f}}(\hat{\mathbf{x}}(t), \hat{\mathbf{x}}^{(1)}(t), \dots, \hat{\mathbf{x}}^{(\nu-1)}(t)) - \mathbf{f}_0(\mathbf{x}(t), \mathbf{x}^{(1)}(t), \dots, \mathbf{x}^{(\nu-1)}(t))\|_2^2 dt \\ &= \int_0^1 \|\hat{\mathbf{f}}(\hat{\mathbf{x}}(t), \hat{\mathbf{x}}^{(1)}(t), \dots, \hat{\mathbf{x}}^{(\nu-1)}(t)) - \hat{\mathbf{f}}(\mathbf{x}(t), \mathbf{x}^{(1)}(t), \dots, \mathbf{x}^{(\nu-1)}(t)) \\ &\quad + \hat{\mathbf{f}}(\mathbf{x}(t), \mathbf{x}^{(1)}(t), \dots, \mathbf{x}^{(\nu-1)}(t)) - \mathbf{f}_0(\mathbf{x}(t), \mathbf{x}^{(1)}(t), \dots, \mathbf{x}^{(\nu-1)}(t))\|_2^2 dt \\ &\lesssim T_1 + \int_0^1 \|\hat{\mathbf{f}}(\mathbf{x}(t), \mathbf{x}^{(1)}(t), \dots, \mathbf{x}^{(\nu-1)}(t)) - \mathbf{f}_0(\mathbf{x}(t), \mathbf{x}^{(1)}(t), \dots, \mathbf{x}^{(\nu-1)}(t))\|_2^2 dt \\ &= O_P(\varsigma_n). \end{aligned}$$

Combining the above we get the desired result.

B Hierarchical Proximal Operator

Algorithm 3 Hierarchical Proximal Operator

Procedure: Hier-Prox(θ, W_0, λ, M)

for $i \in \{1, \dots, r_0\}$ **do**

Sort the entries of $W_{0,i}$ into $|W_{0,i}^{(1)}| \geq |W_{0,i}^{(2)}| \dots \geq |W_{0,i}^{(r_1)}|$

for $j \in \{1, \dots, r_1\}$ **do**

Compute $\omega_j = \frac{M}{1+jM^2} S_\lambda \left(|\theta_i| + M \sum_{k=1}^j |W_{0,i}^{(k)}| \right)$

Find the first j such that $|W_{0,i}^{(j+1)}| \leq \omega_j \leq |W_{0,i}^{(j)}|$

end for

$\tilde{\theta}_i \leftarrow \frac{1}{M} \text{sign}(\theta_i) \omega_j$; $\tilde{W}_{0,i} \leftarrow \text{sign}(W_{0,i}) \min\{\omega_j, |W_{0,i}^{(j)}|\}$

end for

Return: $(\tilde{\theta}, \tilde{W}_0)$

Note:

- r_1 is the number of node in the first hidden layer.
 - $S_\lambda(x) = \text{sign}(x) \max\{|x| - \lambda, 0\}$.
 - We assume $W_{0,i}^{(0)} = +\infty$ and $W_{0,i}^{(r_0+1)} = 0$.
-